A STUDY OF THE PROBLEMS INVOLVED IN THE DETECTION OF MU MESON PAIRS FROM THE MIT SYNCHROTRON

A. JULIAN

1953

A STUDY OF THE PROBLEMS INVOLVED
IN THE DETECTION OF MU MESON PAIRS FROM
THE MIT SYNCHROTRON

by

A. JULIAN
B.S., United States Naval Academy
(1944)

SUBMITTED IN PARTIAL FULFILLMENT
OF THE REQUIREMENTS FOR THE
DEGREE OF MASTER OF
SCIENCE
at the
MASSACHUSETTS INSTITUTE OF
TECHNOLOGY
June, 1953

Signature of Author.....................................
Department of Physics, 22 May 1953

Certified by...
Thesis Supervisor

Accepted by..
Chairman, Departmental Committee
on Graduate Students

A STUDY OF THE PROBLEMS INVOLVED
IN THE DETECTION OF MU MESON PAIRS FROM
THE MIT SYNCHROTRON

by

A. JULIAN

SUBMITTED TO THE DEPARTMENT OF PHYSICS
ON 25 MAY 1953 IN PARTIAL FULFILLMENT
OF THE REQUIREMENTS FOR THE DEGREE OF
MASTER OF SCIENCE

In an attempt to relate the mu meson to the quanta of the nuclear force field, Wentzel has proposed a theory in which the pi meson is essentially a quantum state of a mu meson pair. Because of the anticipated low cross section for the process, and the low efficiency for detection of pair production, a study of the detection problem was needed before a meaningful experiment could be undertaken.

The general detector requirements have been anaylized, and a high efficiency detector manifold has been designed and constructed.

The detection efficiency, and expected counting rates for pair production by either the Wentzelian process, or an electromagnetic process, have been calculated for several target elements.

Response tests have been made of the fast 6BN6 coincidence circuit, and of the Model 402 distributed amplifiers, preliminary to their use in the experiment.

A preliminary set of experiments, with modified detector systems, has been conducted in the Synchrotron beam to resolve shielding, collimation, and background problems. From these experiments, an upper limit has been established for the Wentzel production cross section at 2.5×10^5 times the electromagnetic cross section. This is about the same limit established by Martinelli and his co-workers at the University of California.

Final assembly and bench testing of the detector system is currently underway, in anticipation of an early run with the Synchrotron.

Thesis Supervisor..............................Bernard T. Feld
Professor of Physics

TABLE OF CONTENTS

CHAPTER		PAGE
I.	INTRODUCTION TO THE PROBLEM................	1
II.	DETECTION IN GENERAL......................	4
III.	DETECTOR DESIGN..........................	8
IV.	DETECTION EFFICIENCY.....................	14
V.	EXPECTED YIELDS..........................	22
VI.	ELECTRONICS..............................	29
VII.	EXPERIMENTS IN THE SYNCHROTRON BEAM........	43

BIBLIOGRAPHY.. 50

APPENDIX A - DETAILS OF DETECTOR CONSTRUCTION...... 51

Figure 1 - Detector Body..................
Figure 2 - Phototube Mounts...............
Figure 3 - Housing and Shielding..........

APPENDIX B - ORDER OF MAGNITUDE ESTIMATE OF THE NUMBER OF EFFECTIVE PHOTONS AT THE PHOTO-CATHODE, PER MEV LOST...................... 54

APPENDIX C - APPROXIMATE CALCULATION FOR EFFICIENCY FACTOR η...................... 57

APPENDIX D - TABLE V-1 - Values of the electromagnetic process meson pair production integral from graphical integration........ 64

TABLE V-2 - Electromagnetic process cross section for mu meson pair production as a function of quantum energy............ 65

APPENDIX E - DIAGRAMS, GRAPHS AND TABLES........... 66

Figure 1, 2 - Optical ray diagrams illustrating the reflections in the detector system.................................. 66

Graph IV-1 - Energy Distribution of meson pairs, extrapolated from electron pair kinematics............................ 67

Graph V-1 - Linear Absorption Coefficient in Target Materials at the Higher Quantum Energies.... 68

Graph V-2 - The Electromagnetic Process Meson pair production integral $I^{*} = \frac{1}{3}(k-2)^{3}\left(\frac{2}{k}\right)^{3}\frac{dk}{k}$ 69

Graph VI-1 - 6BN6 Response Testing: Coincidence Pulse Positive Overshoot vs Bias.................... 70

Graph VI-2 - 6BN6 Response Testing Rise Time of Coincidence Pulse vs Bias......................... 70

Graph VI-3 - 6BN6 Response Testing Coincidence Pulse Length vs Limiter Bias...................... 71

Graph VI-5 - 6BN6 Resolving Time Ra-Gamma Test..... 72

Graph VI-6 - 6BN6 Resolving Time Cosmic Ray Test... 72

Graph VI-8 - 6BN6 Resolving Time Synchrotron Test.. 73

Graph VI-9a - Discriminator Action of 6BN6 Coincidence Counting Rate vs Quadrature Grid Bias.... 74

Graph VI-9b - Discriminator Action of 6BN6 Coincidence Counting Rate vs Limiter Grid Bias....... 75

Graph VI-9c - Discriminator Action of 6BN6 Coincidence Counting Rate Cutoff vs Input Pulse Height; Parameter Quadrature Grid Bias............. 76

CHAPTER I

INTRODUCTION TO THE PROBLEM

Experiment indicates that mu-mesons are not produced, singly, in nuclear interactions, although pi mesons can be produced, and with relatively high cross-sections. The appearance of the mu has always been traced to the decay of a parent pi meson. Moreover, the pi meson has been observed to interact strongly with nucleons, while insignificant nuclear interaction is known to occur with single mu mesons.

However, these observations do not necessarily mean that the mu meson is completely unrelated to the quanta of the nuclear force field. Wentzel has proposed a theory in which the pi meson is essentially a quantum state of a mu meson pair (muon--antimuon).[1] In this theory, the nuclear interaction, and creation, of a single mu meson is expected to be very small. However, Wentzel has suggested that a consequence of the excitation of the nuclear field would be an appreciable production of mu meson pairs (as compared, for instance, to single pi mesons).

It is to be observed that it should also be possible to create mu meson pairs, with photons of adequately high energy, by an electromagnetic process analagous to Dirac electron-pair production.[2] (Such an event assumes the mu to be a Dirac particle.)

---

[1] Wentzel, , P.R. 79, 710, (1950)

[2] Dirac, P.A.M., Quantum Theory.

CHAPTER I

INTRODUCTION TO THE PROBLEM

Experiment indicates that mu-mesons are not produced, singly, in nuclear interactions, although pi mesons can be produced, and with relatively high cross-sections. The appearance of the mu has always been traced to the decay of a parent pi meson. Moreover, the pi meson has been observed to interact strongly with nucleons, while insignificant nuclear interaction is known to occur with single mu mesons.

However, these observations do not necessarily mean that the mu meson is completely unrelated to the quanta of the nuclear force field. Wentzel has proposed a theory in which the pi meson is essentially a quantum state of a mu meson pair (meson--antimeson).[1] In this theory, the nuclear interaction, and creation, of a single mu meson is expected to be very small. However, Wentzel has suggested that a consequence of the excitation of the nuclear field would be an appreciable production of mu meson pairs (as compared, for instance, to singly pi mesons).

It is to be observed that it should also be possible to create mu meson pairs, with photons of adequately high energy, by an electromagnetic process analogous to Dirac electron-pair production.[2] (Such an event assumes the mu to be a Dirac particle.)

---

[1] Wentzel, . . P.R. 79, 710, (1950)

[2] Dirac, P.A.M., Quantum Theory.

In order that an attempt to observe these processes be meaningful, a quantitative analysis of the detection problem was needed in view of the possibility that the Wentzelian cross-section may be very small.[3]

This paper presents such an analysis with emphasis on detector design. The various factors entering into detection efficiency are explored to indicate optimum geometries, and a new type of detector has been constructed to realize the optimum efficiency as closely as possible.

Meson electronics, already on hand, have been adapted, with some modifications, to this experiment. Data have been taken to establish the functioning of the electronics, and to resolve shielding and housing problems.

The calculation of expected counting rates has been carried forward in some detail for the electromagnetic process as well as the Wentzelian, in order to provide a good comparison of the relative weights of each at the quanta energies available in the MIT Synchrotron beam. Appropriate extrapolation to other Synchrotron energy spectra and intensities can easily be made.

Detection of either mode of production would be significant, and in particular the Wentzelian, which might reveal the respective roles of the pi and mu in nuclear interactions.

One previous attempt has been made to detect mu pairs--by Mather, Martinelli, and Jarmie with the University of California 322 Mev Bremsstrahlung. Their experiment suffered from very high backgrounds, and detector blocking, due to high electron

[3] Suggested by Dr. A. Wattenberg and Dr. B.T. Feld of the MIT Synchrotron Laboratory.

fluxes, but they were able to assign an upper limit to the Wentzelian production cross-section as 2×10^5 larger than the expected electromagnetic cross section.[4]

---

[4] Mather, Martinelli and Jarmie, UCRL 1166 W 7405-eng-48, University of California.

CHAPTER II

DETECTION IN GENERAL

The proposed experiment involves the detection of mu meson pairs produced by the Bremsstrahlung of the MIT Synchrotron interacting with a suitable target.

With the existing electronics, detection of a single mu meson depends on a delayed coincidence between the meson pulse and the decay electron pulse. Detection of a pair of mesons will involve some type of final coincidence between the delayed coincidence pulses of each meson.

To measure the pair production, a certain basic geometry is envisioned. Figure 2-1, illustrates this geometry and the associated essential electronics in block diagram.

Desirable features for the measurement are as follows:

1. The separate meson signals must be in fast coincidence: a) to reduce the accidentals rate from the high flux of electrons and other particles at the detector positions; and b) to improve their cognizability.
2. For highest efficiency, all mesons with enough energy to leave the target and pass into either detector must be required to decay in the detector. The greatest meson range must lie within the meson detector dimensions. In other words, the detector should be as long as practicable.

FIG. 2-1

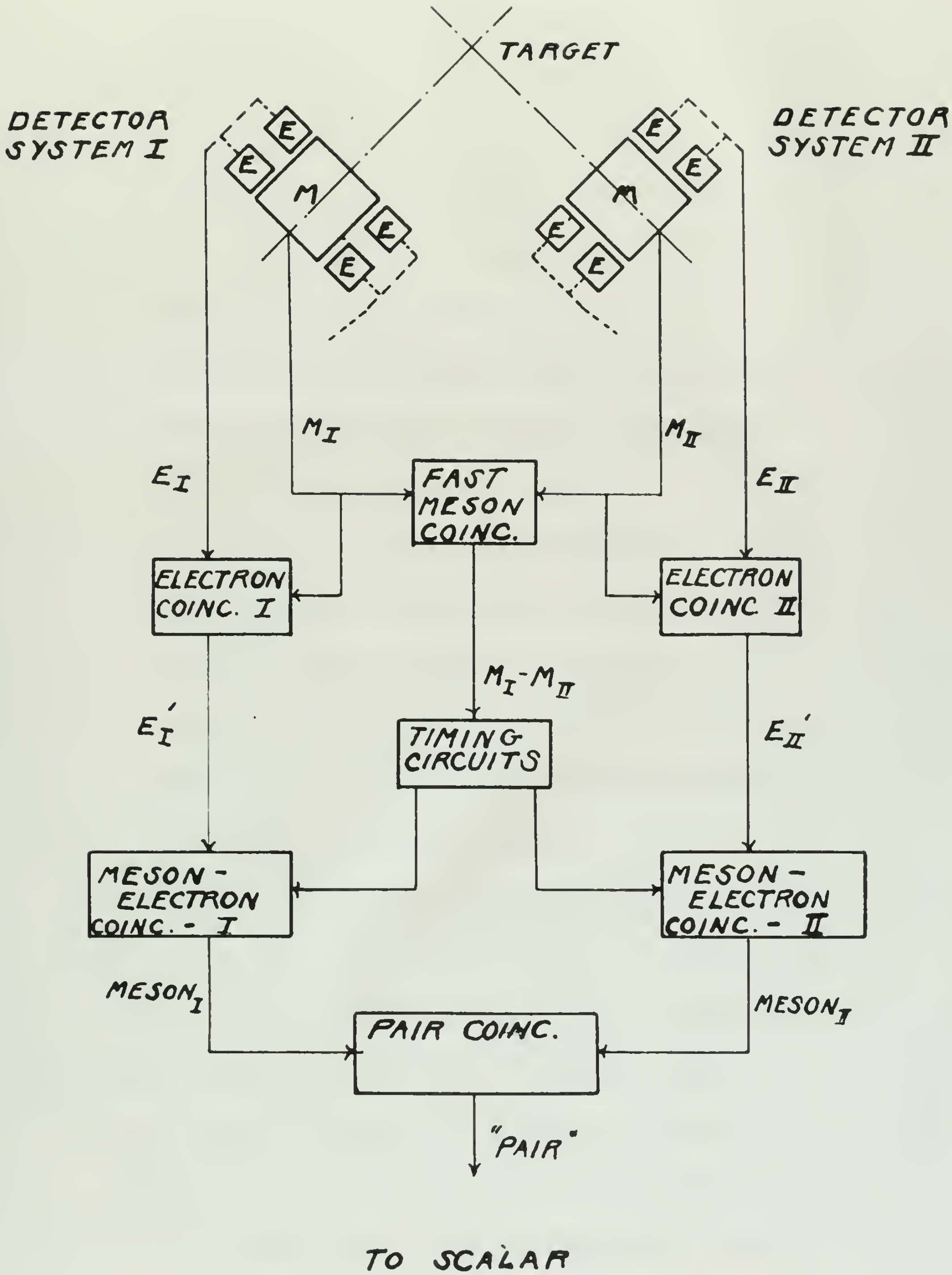
TARGET
DETECTOR SYSTEM I
DETECTOR SYSTEM II
E
M
MI
MII
EI
EII
FAST MESON COINC.
ELECTRON COINC. I
ELECTRON COINC. II
MI-MII
EI'
EII'
TIMING CIRCUITS
MESON - ELECTRON COINC. - I
MESON - ELECTRON COINC. - II
MESONI
MESONII
PAIR COINC.
"PAIR"
TO SCALAR

3. The decay electron (mean life ≈ 2 microsec) must be observed in detectors physically separated from the meson detector to preclude ambiguity in meson and electron pulses in cases of very fast decay, and to negate the effects of phototube "after pulsing." It also appears desirable to require the electron to make coincidence between the meson and the separated electron-detector to keep accidentals rates down.
4. A delayed coincidence must be required between meson-coincidence pulse (1 above) and the electron coincidence pulse (3 above) to verify the identity of the particles. For single mu meson lifetime measurements the delayed coincidence will use timed gate techniques to provide decay time data.
5. A final coincidence is required between the individual delayed-coincidence meson pulses to establish the pair count.

An analysis of the basic requirements listed above shows that, apart from the electronics of the problem, the critical factor in determining success will be in the detector manifold use in the experiment. Experimental difficulties that have been encountered by previous workers (Martinelli et al[5]), and the requirements just mentioned, are, of course, a result of the anticipated very low cross section for mu pair production with the available quanta energy and intensities.

---

[5] Ibid.

These may, for emphasis, be grouped into three major categories:

A. Small effective solid angles for the detection of the pair process. The detection efficiency decreases with the product of the solid angles of each system.

B. Low efficiency of the decay electron detectors in detecting the meson decay in a tandem or side-by-side geometry with the meson detector.

C. High fluxes of particles, other than mu's, producing high singles rates in the electron and meson counters. In Martinelli's experiment, the electron singles rates flooded his decay electron circuits and contributed heavily to his accidental rate. These rates probably were not only large angle pair-electrons and scattered-in electrons from the target, but also photoprotons, and pi mesons. In any event, as he pointed out, reduction of this cause of accidentals rate must begin with shielding of the electron detectors. And they must be shielded, not only from the target, but from showers produced by the beam (or its penumbra) in the shielding material and collimators.

The problems indicated above are discussed in the following chapters:

Chapter III	Detector Design
Chapter IV	Detection Efficiency
Chapter V	Expected Yields and Counting Rates

CHAPTER III

DETECTOR DESIGN

Single nuclear-reaction-product particles generally have a distribution in energy and solid angle. The counting rate from such a reaction is given by:

$$CR \propto \Delta\omega \cdot \Delta E \cdot F \qquad III-1$$

where $\Delta\omega$ is the fractional solid angle;

ΔE is the fractional spectrum energy;

F is the fraction counted (an efficiency factor)

For pair detection, simultaneous events in physically separated and distinct detectors are involved. The counting rate from a pair production reaction is then given by:

$$CR_{pair} \propto \Delta\omega_1 \cdot \Delta\omega_2 \cdot \Delta E_1 \cdot \Delta E_2 \cdot F_1 \cdot F_2 \qquad III-2$$

if there is no correlation in energy or angle between the two emitted particles!

Maximum counting rates result from maximizing the effective solid angle of each detector, both by decreasing detector distance, and increasing detector area. For example, a decrease in the effective detector-target distance from 35cm to 20cm, increases the solid angle factor for this two particle process by about 9. This particular improvement is so significant that special efforts were made to realize it. Further, to obtain as large a value as possible for η[6] (discussed later)

[6]The factor η is the fraction of the total number of decay electrons, from mesons stopped in the inner detector, which are capable of being detected in the outer detector. See Chapter IV on Detection Efficiency for a discussion of η.

CHAPTER III

DETECTOR DESIGN

Single nuclear-reaction-product particles generally have a distribution in energy and solid angle. The counting rate from such a reaction is given by:

$$CR \propto \Delta\omega \cdot \Delta E \cdot F \qquad \text{III-1}$$

where $\Delta\omega$ is the fractional solid angle;

ΔE is the fractional spectrum energy;

F is the fraction counted (an efficiency factor)

For pair detection, simultaneous events in physically separated and distinct detectors are involved. The counting rate from a pair production reaction is then given by:

$$CR_{pair} \propto \Delta\omega_1 \cdot \Delta\omega_2 \cdot \Delta E_1 \cdot \Delta E_2 \cdot F_1 \cdot F_2 \qquad \text{III-2}$$

if there is no correlation in energy or angle between the two emitted particles!

Maximum counting rates result from maximizing the effective solid angle of each detector, both by decreasing detector distance, and increasing detector area. For example, a decrease in the effective detector-target distance from 35cm to 20cm, increases the solid angle factor for this two particle process by about 9. This particular improvement is so significant that special efforts were made to realize it. Further, to obtain as large a value as possible for η[a] (discussed later)

[a] The factor η is the fraction of the total number of decay electrons, from muons stopped in the inner detector, which are capable of being detected in the outer detector. See Chapter IV on Detection Efficiency for a discussion of η.

it is necessary that the decay electron detector have as large a solid angle as possible.

The latter consideration suggested a modification of the type of detector, first used at the MIT Synchrotron Laboratory by J.S. Clark, L.S. Osborne, and Y. Goldschmidt-Claremont in their meson experiments. The model is an inner-cylindrical detector, with a peripherally-contiguous outer cylinder; figure 3-1 illustrates this detector, which was used in the first experimental runs to line up the electronics. Such geometry is quite efficient for observing particles (decay electrons) in the outer detector which originate in the center detector.

The axial length of this design is determined by the upper limit of the mu energy spectrum that can be obtained with the maximum quanta energy available. This limit is reduced by the energy needed by the companion meson to just enter the second detector. The first modification, figure 3-2 , shows the increase in length to this upper limit.

The basic design is purely cylindrical. The effective solid angle per detector, for this cylindrical geometry, can be taken as a crude estimate to be the solid angle subtended by the detector at mid-length. In other words, for a 30 cm long cylindrical system of diameter 4", with the detector face at 20 cm from the target, the effective solid angle is taken to be that subtended at the detector midpoint, 35 cm from the target. For this untapered cylinder, however, it is impossible to attain an effective detector distance of 20 cm because the

FIG. 3-1

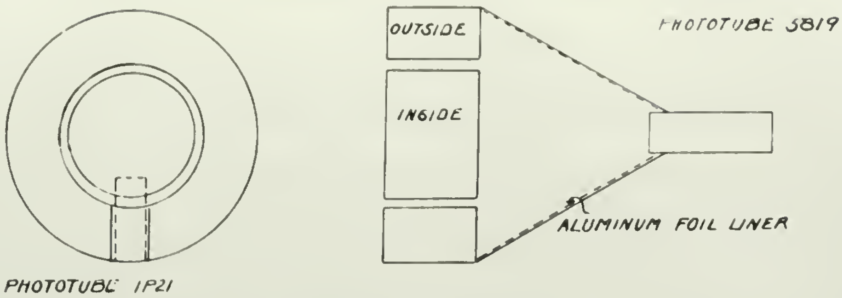

"CLARK" DETECTOR

FIG 3-2

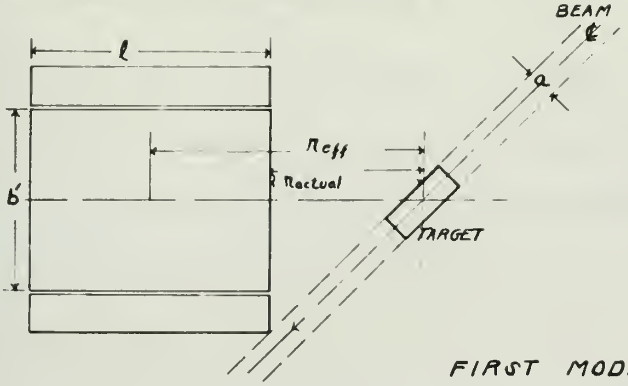

REQUIRING MINIMUM CLEARANCE, a/2 FIXES THE MINIMUM r_{eff} AT 45°. SHIELDING WILL FURTHER INCREASE THE DISTANCE.

FIRST MODIFICATION

FIG 3-3

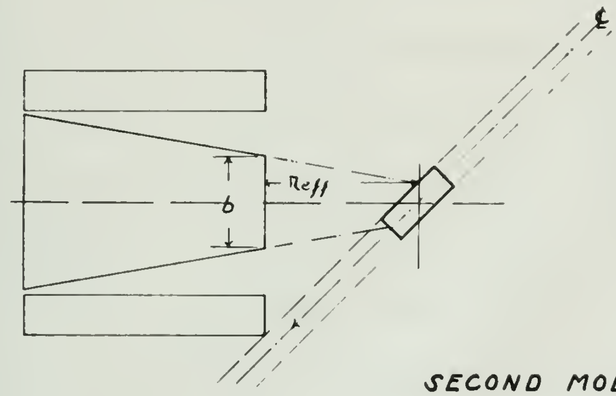

NOTE HOW FRUSTRUM CONSTRUCTION REDUCES r_{eff} TO r_{actual}. FOR "b" = "b'", FIG 3-2, THE PHYSICAL DISTANCE OF THIS GEOMETRY IS GREATER THAN 3-2 FOR SAME CLEARANCE RESTRICTIONS, BUT WITH A NET DECREASE IN r_{eff}.

SECOND MODIFICATION

FIG 3-4

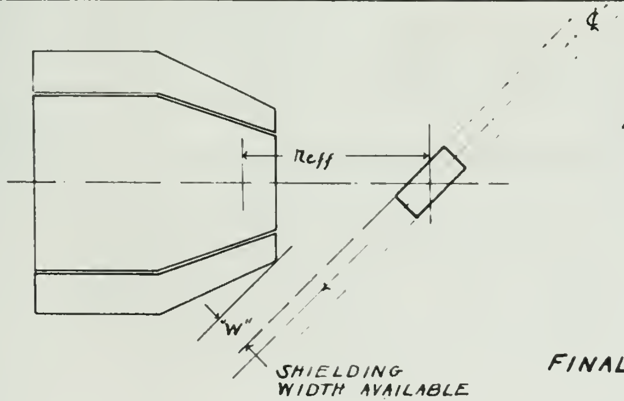

THE OUTER FRUSTRUM GEOMETRY ALLOWS FOR CLOSER ACTUAL DISTANCE AND INCREASE IN SHIELDING WIDTH, "W". A SLIGHT INCREASE IN r_{eff} FROM OPTIMUM, 3-3, IS ACCEPTED AS SPACE AND WEIGHT SAVINGS.

FINAL MODIFICATION

edge of the detector system will be in the beam. Figure 3-2 demonstrates the requirements for minimum beam clearances, and the difficulty encountered with the rectangular cross section.

Forming the inner half of the inner detector as a conical frustrum of appropriate angle, effectively moves the detector towards the target by 15 cm, since the solid angle throughout is now that subtended at the face. Figure 3-3 illustrates such a detector with the resulting conditions imposed.[7] Note that, despite the decrease in the effective detector distance, the factor η has suffered in the critical forward section of the grouping because of the separation of the two detectors in this configuration.

A final modification to allow actual use of the system at 20 cm, and to preserve the factor η necessitated that the outer cylinder also be formed of conical frustums. Details of the final design geometry are shown in figure 3-4 and appended as Appendix A. The physical distance from the detector front-face to the target center is about 20 cm. To make r_{eff} equal to r_{actual}, the inner detector, in this case a continuous conical frustrum, would have had a base diameter of some 25 cm, and a volume of some 8 liters--the outer detectors in turn would be tremendous, an unwieldy and heavy apparatus requiring a large number of phototubes for reasonable photo efficiency and an immense amount of liquid. As a compromise, the frustrum extends to half length only, resulting in a reduction in weight and

---

[7]The scale of figure 3-3 is not the same as the scale of figure 3-2. Dimensions b and b′, the inner detector window diameter, are actually equal.

volume of liquid scintillator by about 45%, and reducing the number of phototubes required.

We do not gain the full increase of 9 in the solid angle factor $\Delta\omega^2$, mentioned in the early paragraphs of this Chapter. Instead, the actual net gain is about 6.5.

Another advantage to the outer frustrum design is that it permits heavier shielding of the system against electromagentic production at small angles, without sacrificing the r_{actual} of 20 cm thus attained.

The sides and end window of the inner detector are made of 20 mil brass, as is the inner wall of the outer detector. The forward end plate, and the outer wall of the outer detector are made of 1/16" brass to give strength and rigidity to the entire structure. The back plates of both detectors are made of 3/8 inch brass. The interior of each is lined with 2 mil aluminum foil as a reflector. All seams were soft soldered at rolled joints, except for the back plate junction which was a combination butt-lap joint to the siding. The back plates contain the liquid filling and vent holes, and the plastic phototube mountings.

Six 5819 photomultipliers are used with each system: two, mounted parallel with the cylinder axis, in the inner detector; and four, mounted at 90° to each other on the circumferential center line of the outer detector back plate. Attached mounts of plexiglass hold the phototube to the back plates in such a way that the photocathode surface is at the surface of the back plate, and is separated from the scintillator

liquid by 1/16 inch of plexiglass and an optical contact of Dow-Corning "200 fluid," a viscous silicone. Some consideration was given to direct liquid contact with the phototubes, but sealing between the glass envelope and the brass has not been found reliable. It is for this reason that the full plastic envelope was used. Rubber "O" ring seals maintain the viscous oil reservoir between the tube and the plastic, and act as a mechanical clamp to hold the phototube in position. A small hole near the base of the flange of the plastic mounting allows for venting of surplus viscous oil during tube insertion. The simple contact seal between the back plate and the plexiglass tube-mounting provides the liquid seal for the cyclohexylbenzene containers. Figure 2, Appendix A shows details of the fitting and mounting.

Besides making possible the 20 cm target distance, the frustrum construction increased the photon collection efficiency for the liquid system because of the funneling of successive reflections toward the large end of the cones. Ray diagrams, figures 1 and 2, Appendix E illustrates this effect.

An order of magnitude calculation of the number of effective photons collected (those producing secondary electrons on the photo-cathode) per Mev lost in the liquid indicates an expected average of about 10 per Mev. A minimum ionizing electron at radial passage through the thinnest part of the outer detector will lose about 4 Mev, to produce an expected 40 effective (3 ev) photons in the outer detector.

liquid or 1/16 inch of plexiglass and an optical contact of Dow-Corning "200 fluid," a viscous silicone. Some consideration was given to direct liquid contact with the phototubes, but sealing between the glass envelope and the brass has not been found reliable. It is for this reason that the full plastic envelope was used. Rubber "O" ring seals maintain the viscous oil reservoir between the tube and the plastic, and act as a mechanical clamp to hold the phototube in position. A small hole near the base of the flange of the plastic mounting allows for venting of surplus viscous oil during tube insertion. The simple contact seal between the back plate and the plexiglass tube-mounting provides the liquid seal for the cyclohexylbenzene containers. Figure 2, Appendix A shows details of the fitting and mounting.

Besides making possible the 20 cm target distance, the frustrum construction increased the photon collection efficiency for the liquid system because of the funneling of successive reflections toward the large end of the cones. Ray diagrams, Figures 1 and 2, Appendix E illustrates this effect.

An order of magnitude calculation of the number of effective photons collected (those producing secondary electrons on the photo-cathode) per Mev lost in the liquid indicates an expected average of about 10 per Mev. A minimum ionizing electron at radial passage through the thinnest part of the outer detector will lose about 4 Mev, to produce an expected 40 effective (3 ev) photons in the outer detector.

See Appendix B for this calculation.

The detectors are to be mounted at 45° to the beam on each side, and at about 20 cm target to detector-face distance. A beam collimated to 1 inch width will be used. An arbitrary selection of 1 1/2 inches from the beam center-line was taken to be minimum approach distance for any housing material. The method of housing the detectors is shown in figure 3, Appendix A.

CHAPTER IV

DETECTION EFFICIENCY

Equation III-2 must be analyzed in detail, and the correlation between the energy of the emitted particles taken into account.

The detection efficiency of a single detector is:

$$\varepsilon' = \Delta\omega \cdot \delta \cdot \eta \cdot \chi \qquad \text{IV-1a}$$

where $(\delta\eta\chi)$ is the factor F of equation III-1.

The detection efficiency for the pair of detectors is:

$$\varepsilon = 2(\Delta\omega)^2 \cdot \delta^2 \, \eta^2 \cdot \chi \cdot g \cdot f \qquad \text{IV-1b}$$

where the additional factors 2, g, and f, take account of the characteristic physics of the process.[8]

g is a factor which results from the energy correlation between the emitted mesons for the pair process.

$(1-\delta)$ is the fraction of the meson decays which occur during the dead time of the counting circuit after the meson pulse. This dead-time comprises the electronic transit time, and fixed delays in the circuit. δ^2 is the fraction counted of the total pairs of decays after dead time.

χ is the factor relating to the competitive processes of decay and nuclear absorption for negative mu mesons.

η is the fraction of the mesons which decay in a

---

[8]The factor 2 is a statistical one which arises in the following way: Since either meson can be counted in either detector, there are two combinations that will result in a successful detection. Meson 1 in detector 1; meson 2 in detector 2; or meson 1 in detector 2; meson 2 in detector 1.

detector that form a detectable decay electron.

f is a factor that gives the true angular distribution as compared to an uncorrelated spherically symmetric angular distribution.

The value of $\mathcal{E}$ calculated will be a lower limit on the detection efficiency, based on the assumption of absolutely no correlation between the fractional solid angles $\Delta\omega_1$ and $\Delta\omega_2$.

These factors are discussed below in detail.

Factor $\Delta\omega_1 \cdot \Delta\omega_2$

The solid angle product is a very critical part of the efficiency. The basic solid angle geometry is shown in Figure 4-1.

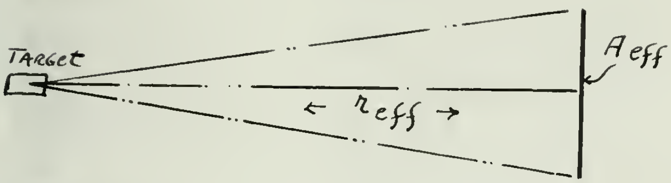

FIG. 4-1.

A_{eff} is the effective detector aperture area.

r_{eff} is the effective detector distance.

Some representative values of $(\Delta\omega)^2$ for various $A_{eff}-r_{eff}$ combinations, which appear reasonable and attainable, are listed in Table .

Table 4-1 ($\Delta\omega$ and $(\Delta\omega)^2$)

A_{eff}/r_{eff}	$\Delta\omega$	$\Delta\omega^2$
80.8/20	1.61×10^{-2}	2.57×10^{-4}
125.8/20	2.51×10^{-2}	6.25×10^{-4}
80.8/35	$.526 \times 10^{-2}$	$.275 \times 10^{-4}$
125.8/35	$.821 \times 10^{-2}$	$.67 \times 10^{-4}$

A = 80.8 cm is the 4 inch diameter

A = 125.8 cm^2 is the 5 inch diameter

Note that an increase in detector diameter by 1" increases the efficiency at either value of A_{eff} by a factor of about 2.4. Decreasing r_{eff} from 35 cm to 20 cm, holding A_{eff} constant, increases efficiency by a factor of about 9.

The path length of the decay electron becomes too large in general, and the factor η^2 decreases, for a detector diameter of more than about 6 1/2 inches. Consequently this was the maximum diameter used in the inner detector, resulting in choosing an aperture diameter of 4 inches (A_{eff}=80.8 cm^2). The value of $(\Delta\omega)^2$ for this A_{eff}-r_{eff} combination from Table 4-1 is 2.57×10^{-4}.

Factor δ^2

The transit time of the circuit is negligibly short compared to the fixed delay time in the meson electronics. The meson coincidence pulse triggers the electron-meson gate after a 1/2 microsec fixed delay. The 1/2 microsec delay is used to preclude false coincidences in the gate circuit due to slowing of one or the other pulse in the discriminators. The fraction of all the mesons that decay in 1/2 microsec is:

$$(1-\delta) = 1 - \exp\left(-\frac{t}{\tau}\right) \approx .21 \qquad \text{IV-2a}$$

hence δ^2, the fraction of the total that are observable in pairs, is

$$\delta^2 \approx .79^2 \approx .62 \qquad \text{IV-2b}$$

Note that an improvement in δ^2 can be obtained by decreasing the fixed delay in the electronics to 1/4 microsec in lieu of 1/2 microsec. This results in an increase by a factor, Note that an increase in detector diameter by 1" increases the efficiency at either value of A_{eff} by a factor of about 2.4. Decreasing T_{eff} from 50 ns to 25 ns, holding A_{eff} constant, increases efficiency by a factor of about 2.

The path length of the decay electron becomes too large, in general, and the factor η^2 decreases, for a detector diameter of more than about 6 1/2 inches. Consequently this was the maximum diameter used in the inner detector, resulting in choosing an aperture diameter of 4 inches (A_{eff}=80.2 cm^2). The value of $(\Delta\omega)^2$ for this A_{eff}-T_{eff} combination from Table 4-1 is 2.67×10^{-4}.

Factor δ^2

The transit time of the circuit is negligibly short compared to the fixed delay time in the meson electronics. The meson coincidence pulse triggers the electron-meson gate after a 1/2 microsec fixed delay. The 1/2 microsec delay is used to preclude false coincidences in the gate circuit due to [illegible] of one or the other pulse in the discriminators. The fraction of all the mesons that decay in 1/2 microsec is:

$$(1-\delta) = 1 - \exp\left(-\frac{t}{\tau}\right) \approx .21 \qquad \text{IV-2a}$$

Hence δ^2, the fraction of the total that are observable in pairs, is

$$\delta^2 \approx .79^2 \approx .62 \qquad \text{IV-2b}$$

Note that an improvement in δ^2 can be obtained by decreasing the fixed delay in the electronics to 1/4 microsec in lieu of 1/2 microsec. This results in an increase by a factor,

$\frac{.79}{.62} = 1.27.$

Factor χ

The experiments of Ticho,[9] and Conversi et al,[10] have shown that the negative mu meson is frequently absorbed in high Z materials instead of decaying. For the purposes of this experiment, absorption of a negative mu meson will result in a lost pair count, since counting depends on the production and detection of the decay electrons.

For our absorber (the scintillator liquid) the average Z is about 4.

The results of Sigurgeirsson and Yamakawa[11]--relative number of decay electrons per stopped meson--are statistically about the same for Be and C, both being approximately equal to unity. For our calculations, the factor χ is therefore taken to be 1.

Factor η^2

The decay electrons have a distribution in energy, consequently a distribution in range, and thus some of them will not reach the outer detector. Due to the shape of the detector, the fraction that reaches the outer detector is a function of the position of the meson decay.

η is the fraction of decay electrons produced in one of the inner detectors that reach the outer detector--and are

[9] Ticho, H.K., P.R. 74, (1337) 1948.

[10] Conversi, Pancini and Piccioni, P.R. 68, 232, 1945, P.R. 71, 209, 1947.

[11] Sigurgeirrson, T. and Yamakawa, K.A., Rev. Mod. Phys. 21, 124, 1949.

observable--averaged over the entire detector.

The value of η is calculated in Appendix C. The basic considerations involving the calculation are given below.

The decay electron spectrum shows a most probable energy of about 30 Mev. Analytic forms for the spectrum energy have been formulated by Hubbard.[12]

The number of decay electrons of energy E in dE is f(E):

$$f(E)dE = dE\,\frac{12E^2}{W^4}\left(W-E+\tfrac{2}{9}\rho[4E-3W]\right) \qquad IV\text{-}3a$$

Taking ρ here to be .25, a value nearly that recommended by Hubbard, and combining the bracket, leads to:

$$f(E)dE = dE\,\frac{12E^2}{W^4}(.83W-.78E) \qquad IV\text{-}3b$$

The bracket may be taken as .8(W-E), whence,

$$f(E)dE = 9.6\,\frac{E^2}{W^4}(W-E)dE \qquad IV\text{-}3c$$

$W=\frac{m_\mu c^2}{2}$; $W \cong \frac{110}{2}$ = 55 Mev, the maximum kinetic energy that the electron may carry off from the decay.

A rigorous determination of the fraction of the decay electrons that leave the meson detector--with enough energy to produce a pulse in the electron detector--involves a complicated three-space-energy integration over the volume of the detector and throughout the spectrum.

A reasonable approximation has been made to the evaluation of η, taking into consideration the depth of penetration of the meson, and the electron spectrum. The detailed calculations (Appendix C) give for the value:

$$\eta = .609; \quad \eta^2 = .37$$

---

[12] Hubbard, H.W., Thesis University of California, 10 March 1952, "Positron Spectrum from decay of mu mesons."

Factor g

Factor g is the fraction of the total pair production of mesons accepted in the detector system, as a function of the distribution of the available kinetic energy. The energy distribution is such that an unequal division of energy is much more probable than an equal division.

If the division of kinetic energy is such that one meson carries off enough energy to stop at the back wall of one very long detector, and decay, the other meson may not get out of the target. The pair is not counted. For a short detector, the high energy particle of the pair may pass through the detector without stopping and decaying--the result is again a lost count.

Graph IV-1, Appendix E, energy distribution of meson pairs, extrapolated from similar distributions for the electron pair kinematics, has been plotted as a piecewise linear approximation, symmetric about the fraction one-half.[13]

Superimposed on these approximate curves are the energy acceptance limits imposed by: the target thickness to the exiting mu; the absorber thickness; and the meson detector front window thickness. As a not entirely arbitrary choice of these parameters, consider a target of thickness one inch transverse to the beam, with 1/4 inch of lead absorber, and a window of .02 inch brass. The limits of energy acceptance are determined by: $[E_\gamma - 2 m_\mu c^2]$ minus the energy loss in

$$[\sqrt{2}'' \text{ target} + \tfrac{1}{4}'' Pb + .02'' \text{ brass}] = T_o - T_L$$

---

[13] Heitler, W ., Quantum Theory of Radiation.

For each value of k_{max} (E_{max}), the acceptance limits are at T_{ℓ}, $T_o - T_{\ell}$; the fraction of the total area under the distribution curve bounded by T_{ℓ} and $T_o - T_{\ell}$ is the maximum fraction of the total mu pair spectrum that is observable in the whole solid angle.

Note that at lower photon energies the acceptance fraction becomes very small. The combination: cross-section; number of photons in the energy range; and acceptance fraction in the energy range, probably tends to make the likelihood of an observation of a pair from either group (those from photons in the highest energy region, as opposed to those from photons in an intermediate or low region) about equal, other factors remaining unchanged.

Taking an average over the range of k, we have:

$$g \approx .75 \qquad \text{IV-5}$$

Factor f

To conserve momentum and energy for pair production from a single nucleon, the mesons will tend to be emitted in the forward direction. Since only the forward hemisphere is involved, the factor f is about 4, and probably greater. (See discussion on upper limit efficiency, latter part of this section.)

$$f \approx 4 \qquad \text{IV-6}$$

The lower limit of the total detection efficiency factor then becomes:

$$\varepsilon = 2 \cdot \Delta\omega^2 \cdot d^2 \cdot \eta^2 \cdot x \cdot g \cdot f$$

$$\varepsilon = 2 \times 2.57 \times 10^{-4} \times .62 \times 1 \times .37 \times .75 \times 4$$

$$\varepsilon = 3.53 \times 10^{-4} \qquad \text{IV-7}$$

The use of this lower limit efficiency is a reasonable approach to the problem of the Wentzel production, since we have no knowledge of the correlative effects of the assumed meson field.

However, for the electromagnetic production discussed in the later parts of Chapter V following, an increase in the expected counting rate figures may be obtained. The yield calculations for the electromagnetic process are made assuming a completely incoherent process, (linear Z dependence). If calculation can show a Z dependence of the type: $Z + Z^2 \times$ (Form factor), that is, with additional coherent production over the nucleus, the expected counting rate values will be increased. In this case there is a strong forward correlation of the mu pairs; 1) from the theoretical cross-section (Heitler) for Dirac particle pair production; and, 2) from the coherence in the forward direction. Both of these will make the factor <u>f</u> greater than 4 for particle detection at forward angles.

CHAPTER V

EXPECTED YIELDS

Introduction: In order to calculate the counting rate to be expected, one needs a knowledge of the cross section. Lacking a knowledge of the cross section all one can do is express the Counting rate as a function of the integral of the cross section over the energy range available. If a CR is observed, experiments at different energies could give the energy dependence of the cross section. In this section, the general expression for the counting rate as a function of the integral cross section is developed.

The yield of the pair production process can be written in differential form as:

$$d^2Y = d\phi(E)\, N\, \sigma(E)\, dx \qquad \text{V-1}$$

where d^2Y is the yield, in meson pairs per unit target length, per unit quantum energy interval, per mouse.[14]

$d\phi(E)$ is the number of quanta having energy between E and E dE over the entire target area, per mouse.

---

[14] The "mouse" unit is a Laboratory unit of integrated intensity. The beam is monitored in an ionization chamber at the collimator face. Charge accumulated in the chamber is discharged after 7×10^7 e.q. (See S.M. Thesis H. Ratz.) Note that even though the collimation to one inch absorbs some of the quanta produced in the Synchrotron target, the rate, e.q. per mouse at the target position will still be a, since the ionization chamber is on the target side of the wall. The collimation effect will be to increase the running time per mouse.

N is the number of target atoms per cm^3.

$\sigma(E)$ is the cross section for meson pair production at energy E, per target atom.

The number of quanta per mouse in the energy interval E to E + dE, d ϕ (E), is a function of the target length:

$$d\phi(E) = d\phi_0(E)\,e^{-\mu x} \qquad V\text{-}2$$

whence, $$dY = N\sigma(E)\,d\phi_0\int_0^{l} e^{-\mu x}\,dx \qquad V\text{-}3$$

where dY is the yield in meson pairs per unit quantum energy interval in target length l[15]

and $$dY = N\sigma\,d\phi_0\left(\frac{1-e^{\mu l}}{\mu}\right). \qquad V\text{-}5$$

or $$dY = N\sigma\,d\phi_0\,l_{eff} \qquad V\text{-}5$$

where l_{eff} is the effective target length, values of which[16] for several elements are tabulated in Table 5-1

Table 5-1 - Effective Target Length (cm)

Be	9.23	Al	7.01
C	8.96	Cu	2.48

Now $$d\phi_0 = \frac{\text{Target area}}{\text{Beam area}} \times \alpha\frac{dE}{E} = \alpha'\,d(\ln E) \qquad V\text{-}6$$

---

[15] Collimation determines the useful target length to be 4 inches.

[16] The figures in Table 5-1 are calculated, taking μ equal to the asymptotic pair limit coefficient.[17] Graph V-1, Appendix E, Linear absorption coefficient for the elements listed in Table 5-1 shows that this assumption is reasonably valid at the energies under consideration.

[17] Fermi, E., Nuclear Physics.

where $\alpha = 7 \times 10^7$ equivalent quanta (e.q.) per mouse in the MIT beam;

$\frac{dE}{E}$ is the energy spectrum of the Bremsstrahlung;[18]

α' is the e.q. per mouse, corrected for the actual area, and is equal to:

$$\alpha' = \frac{2}{\pi} \times 7 \times 10^7 \text{ e.q. per mouse}$$

therefore $Y = N\, l_{eff}\, \alpha' \int_{E_{MIN}}^{E_{MAX}} \sigma(E)\, d(\ln E)$

or $Y = N\, l_{eff}\, \alpha' I$ (events per mouse)[19] V-7

The limits of integration are somewhat variable: The upper limit is a function of the Synchrotron, with a probable maximum of 340 Mev. The absolute lower limit is the threshold energy for the pair process (215 Mev). The practical lower limit is a function of target and absorber material and thickness.[20]

The observable yield (Counting Rate) is then:

$$CR = \epsilon Y = \epsilon N l_{eff}\, \alpha' I \qquad \text{V-8}$$

The expected counting rate, in counts per mouse, is tabulated in Table 5-2 for the four elements C, Be, Al and Cu, as a function of the integral I. (The integral has the dimensions, cm^2.)

---

[18] The spectrum has been theoretically predicted, and experimentally verified, as actually being about: $.87 \times \frac{dE}{E}$.

[19] To determine the rate, "events per equivalent quanta," divide the rate "events per mouse" by $2/\pi \times 7 \times 10^7$.

[20] To reduce background, it was found necessary to put 1/4 inch of lead in front of the detector--see Chapter VII.

Table 5-2 Expected counting rate (counts per mouse)

Be - 1.783×10^{28} I	Al - $.66 \times 10^{28}$ I
C - 1.126×10^{28} I	Cu - $.718 \times 10^{28}$ I

The practical upper limit for the length of a run was taken to be about 10^5 mice.[21] So unless the integrated cross section, I, is of the order of 10^{-33} cm^2, or greater, it is probable that no pair production will be detectable.

If a few 10^5 mouse runs are completed with no counting established, it will be possible to fix the upper limit of the Wentzelian cross section at near 10^{-33}, an improvement over Martinelli's limit by about 10^6.

The expectation counting rate for electromagnetic mu pair production can be calculated by substituting the theoretical cross section in the above relationships.

P.V.C. Hough[22] has developed formulae based on the Bethe-Heitler[23] equations for electron pair production which are represented to give better fit to experimental data than the latter. In particular, for symmetrical division of the kinetic energy, his equations give:

$$\sigma_{pair} = .785\,\sigma_0$$
$$\sigma_0 = .085 \cdot \frac{1}{137}\left(\frac{Ze^2}{mc^2}\right)^2 \qquad \text{V-9}$$

At energies very slightly above threshold, Hough's best power law approximation gives:

---

[21] This limit is set by considerations of the backgrounds observed in the preliminary study--see Chapter VII.

[22] Hough, P.V.C., P.R. 73, 1 February 1948.

[23] <u>Ibid</u>.

$$\sigma_0 = \frac{1}{3}(k-2)^3\left(\frac{2}{k}\right)^3 \text{ in units of } \frac{1}{137}\left(\frac{Ze^2}{mc^2}\right)^2 \qquad \text{V-10}$$

$$k = \frac{h\nu}{mc^2}; \; (k \ll 1)$$

which equation is 12% low at k = 3, with increasing error as k becomes much greater than 1.

Extrapolating the equations to the mu pair process by introducing the meson mass, gives:

$$\sigma_{\mu\, pair} = .785 \left[\frac{1}{3} (k-2)^3 \left(\frac{2}{k}\right)^3 \right] \text{ in units of } \frac{1}{137}\left(\frac{Ze^2}{m_\mu c^2}\right)^2 \qquad \text{V-11}$$

From the mass ratio alone, this hypothetical cross section is down at once by a factor of about 4×10^4 from the electron pair cross section. Moreover, the square Z dependence implies a coherence which is probably not valid for the meson production. It is probably more realistic, and does not change the order of magnitude, to take the Z dependence as linear.[24]

The expected counting rate is:

$$CR = \varepsilon N \, l_{eff} \, \alpha' I' \qquad \text{V-12}$$

where $I' = C\int \sigma \, d(\ln E)$ can now be evaluated;

$$I' = C\int_{k_{min}}^{k_{max}} (k-2)^3 \left(\frac{2}{k}\right)^3 \frac{dk}{k} \qquad \text{V-13}$$

$I^* = \frac{I'}{C}$ (Graph V-2, Appendix D) is a numeric and has the values tabulated in Table V-2, Appendix D, where the integration is carried out by graphical methods for various combinations of the upper and lower limits. A practicable

---

[24] Table V-1, Appendix D, tabulates the electromagnetic cross section (per Hough with linear Z dependence) as a function of quantum energy.

lower limit, to discount energy loss in the target and the absorber is about 240 Mev.

For E_{max} = 340 Mev. (k_{max}= 3.18), and E_{min}= 240 Mev. (k_{min}= 2.25), I'' corrected for the 12% low error inherent in the Hough formulae, at k = 3, is about .06.

The constant C, here is: (See Table 5-3)

$$C = \frac{.785}{137}\left(\frac{e^2}{m_\mu c^2}\right)^2 Z \qquad V\text{-}14$$

Table 5-3 Constant C (Equation V-14) in cm^2

Be	$- 4.12 \times 10^{-32}$	Al	$- 1.34 \times 10^{-31}$
C	$- 6.18 \times 10^{-32}$	Cu	$- 2.99 \times 10^{-31}$

The expectation counting rate is:

$$CR = (\epsilon N l_{eff} \alpha') \, CI'' \text{ (counts per mouse)} \qquad V\text{-}15$$

where the factor ($\epsilon N l_{eff} \alpha'$) is the coefficient of I in Table 5-2.

Values for this expectation counting rate are tabulated in Table V-4, for these four elements, for various limits of the integral I''.

For the particular case of Berylium between limits of 340 Mev and 240 Mev, the rate is:

$$CR_{BE} = 4.46 \times 10^{-5} \text{ (counts per mouse)}$$

a rate which is of the same order of magnitude as that which we could expect from Wentzelian pair production with an integrated cross section, I, of about 2.5×10^{-33} cm^2. For runs of 10^5 mice, both the Wentzelian rate for this cross section, and

the electromagnetic rate are at the extreme outer limit of our detection probability.

Table V-4 Expectation counting rate for electromagnetic meson pair production in counts per mouse times 10^5.

Lower Limit I"=240 Mev				Lower Limit I"=260 Mev		
Upper Limit	350 Mev	340 Mev	330 Mev	350 Mev	340 Mev	330 Mev
Be	5.35	4.46	3.68	5.11	4.23	3.44
C	5.06	4.22	3.48	4.84	3.99	3.26
Al	6.43	5.36	4.43	6.15	5.08	4.14
Cu	15.59	13.0	10.72	14.9	12.3	10.02

CHAPTER VI

ELECTRONICS

A. Tests of 6BN6 Coincidence - 402 Amplifier Group

The first phase of the actual experimental investigation comprised an analysis of a 6BN6 fast coincidence circuit and associated distributed amplifiers, model 402. Calculation showed that an important part of the solution to a reduction in the background and accidentals rates lay in reducing circuit resolving times to a minimum by taking advantage of fast coincidence circuits where they could be used.

The distributed amplifiers, model 402 were slightly redesigned in the LNSE Laboratory from the Hewlitt-Packard model 460A, which has the following characteristics:

> Maximum output voltage to an open circuit--8 volts; maximum output voltage terminated in 330 ohms--4.75 volts; maximum gain, 20 db (10), using 6AK5 tubes operating at g = 5000 micromhos. The essential differences between the 402 and the H-P 460A are: (a) voltage regulation on the 402; (b) addition of screen circuit decoupling resistances on the 402; (c) slight increase of g_m with the 402; (d) termination in 200 ohms.

Complete circuitry of the amplifier, including regulated power supply are available as LNSE Dwg # D-382-A.

The 6BN6 coincidence circuit used was designed in the

LNSE Laboratory, Dwg B-1801-A. Its essential feature is the use of the 6BN6, gated grid discriminator tube. The plate current-limiter grid characteristic curves show sharp limiting action from a cutoff of about -3 volts for 0 quadrature volts. Operation as a coincidence tube requires positive pulses to both the negatively biased limiter, and quadrature grids. Single-grid plate pulses can be formed for low values of bias, but proper grid voltage adjustment with regard to expected input pulse size enable its use as a coincidence circuit with very short resolving time. The time constants of the grid stages are such that resolving times of the order of 10^{-9} sec are attainable. However, with associated circuitry, especially amplifiers, the resolving time suffers somewhat.

Rather extensive testing of the 6BN6 circuit with the 402 amplifier input was made. Use of this particular combination was predicated on the necessity for an early circuit discrimination against the expected high flux of electrons, protons, neutrons, and pi mesons into the meson detectors. And even with a resolving time of 10^{-9} sec, a flux of 10^3/sec in each detector gives an accidental meson coincidence rate of about .001 per mouse, much too high without the other restrictions placed on the true counting rate described heretofore.

Response testing was done with artificial coincidence pulses (split single pulses) from a lab pulser. Seriously large secondary coincidence pulses, and coincidence overshoot pulses were observed for values of grid biases that were too low. Test curves indicated that secondary and

LVSE Laboratory, Dwg B-1800-s. Its essential feature is the use of the 6BN6, gated beam discriminator tube. The plate current-limiter grid characteristic curves show sharp limiting action from a cutoff of about -3 volts for 0 quadrature volts. Operation as a coincidence tube requires positive pulses to both the negatively biased limiter, and quadrature grids. Single-grid plate pulses can be formed for low values of bias, but proper grid voltage adjustment with regard to expected input pulse size enable its use as a coincidence circuit with very short resolving time. The time constants of the grid stages are such that resolving times of the order of 10^{-9} sec are attainable. However, with associated circuitry, especially amplifiers, the resolving time suffers somewhat.

Rather extensive testing of the 6BN6 circuit with the 40F amplifier input was made. Use of this particular combination was predicated on the necessity for an early circuit discrimination against the expected high flux of electrons, protons, neutrons, and pi mesons into the meson detectors. And even with a resolving time of 10^{-9} sec, a flux of 10^5/sec in each detector gives an accidental meson coincidence rate of about .001 per pulse, much too high without the other restrictions placed on the true counting rate described heretofore.

Extensive testing was done with artificial coincidence pulses (split single pulses) from a lab pulser. Seriously large secondary coincidence pulses, and coincidence overshoot pulses were observed for values of grid biases that were too low. Test curves indicated that boundary was overshoot pulses are negligible only for grid biases more negative than approximately minus 3 volts, on both quadrature and limiter grids. This negative 3 volts corresponds to the beginning of the sharp rise to the limited region of operation. On all subsequent testing, minus 3 volts was taken as the minimum negative limit of valid data. See Graphs VI-1, Appendix E. The coincidence pulse length and rise time appeared to be a function of both biases, but only for long pulser input signals. No remedial measures are necessary for the experiment wherein terphenyl-cyclohexylbenzene pulses of the order of 10^{-9} sec rise time are to be used. (Graphs VI-2, VI-3, Appendix E.)

Similar testing, with Ra-gamma pulses, detected in xylene, and then split for artificial coincidence, reduced to the same qualitative behavior.

GAIN TESTING

The distributed amplifiers, Model 402, were claimed to be capable of producing 10 volt output pulses with an overall maximum gain per amplifier (two stages) of 10.

Controlled gain tests showed that gain through the amplifiers was strongly dependent on input pulse amplitude and rise time, and that saturation output-levels were of the order of 6-7 volts. It appears that for the H-P 460A, the published maximum output voltage terminated is 4.75 volts, while in our amplifier, with an output resistance of 270 ohms, the maximum output voltage (with termination into 200 ohms) is $\frac{200}{270} \times E_{out}(max)$,

and assuming E_{out}(max) to be 10 volts, this makes for $E_{max} \approx 7$-7.5^{V}. This is about what was found to be the case.

The following results were obtained from gain testing. The figures are for identical amplifier stage biases of -1.5 volts, and for input pulse heights of .3 volts. Note that the gain figures for 2 amplifiers in series reflect the saturation output voltage by a reduction in the overall gain, from G^2, to a value consistent with the previously determined maximum output of 6-7 volts.

Table 6-1 shows data for three pulse types:

A. Slowly rising short pulses ($T_r = 2\mu s$; $T_e \approx 2\mu s$)

B. Slowly rising long pulses ($T_r \approx 2\mu s$; $T_e \approx 90\mu s$)

C. Fast rising long pulses ($T_r \approx .1\mu s$; $T_e \approx 120\mu s$)

The length of the short pulse here given is the base length at zero voltage; the important difference between the "short" pulses and "long" pulses here is the pulse shape near the maximum height.

Table 6-1 (Gain of 402 Amplifiers)

	A	B	C
Single	3.75	6.5	18
Cascaded	9.5	-	19

It is necessary to specify the input pulse height because the observed gain was a function of input pulse height

as may be seen from Table 6-2 for type A pulses:

Table 6-2 (402 Amplifier Gain vs Input)

Input Pulse Height	Gain	
.1 volts	4	Single
.3	3.75	Single
1.0	2.4	Single
.05	30	Cascaded
.1	19	Cascaded
.3	9.5	Cascaded
1	4	Cascaded

The input circuit time constant of the 402 amplifier is approximately 2 microseconds, so that the long pulses B and C of Table 6-1 are clipped as fairly flat, 2 microsecond input pulses.

In general, for a single amplifier, gain was found to be highest for a fast rising pulse, with a fairly flat top to the limit of clipping time, as can be seen qualitatively from the increase in gain from A to B to C, wherein these general criteria are more nearly approached.

The experiment at hand will require two 402 amplifiers to amplify each meson signal before the fast coincidence. Resolving time measurements were made to determine resolution of the 402 amplifiers and the 6BN6 circuit. The determination of

resolving time of the complete circuit (amplifiers and 6BN6) was made by introducing various lengths of signal cable in one grid circuit or the other as a delay mechanism. The signal cable used is British 200 ohm, center wire coaxial. Inasmuch as all the available 200 ohm cable was already made up into leads of varying length, a restriction was placed on the amount of delay that could be used. Data points are separated by a time corresponding to the made-up cable lengths. The speed of the cable is negligibly different from the speed of light.

Resolving time data were taken for four different source combinations.

1. Using artificial coincidence (split pulses) from a Ra- source.

2. Using actual coincidences from cosmic rays, in two small volume liquid scintillator detectors.

3. Using actual coincidences from a Co^{60} source.

4. Using actual coincidences in two liquid detectors from events produced by a target in the synchrotron beam.

In each case, the 6BN6 grid biases were set low enough so that single pulses of the expected normal size were inadequate to trigger the coincidence circuit. The observations, of course, were inaccurate to the extent that the biases used allowed high-pulse height single-events to trigger. However, for the lengths of detectors used (small volume), and the bias settings, a very small fraction of the total count at any delay was due to single pulse coincidences.

For each run, the coincidence counting rate was plotted as a function of delay on each grid.

An average of four runs using the Ra source indicated a circuit resolving time of the order of 2-3 x 10^{-8} sec. Graph VI-5, Appendix E is a plot of the average, normalized counting rate vs delay for the four runs. Clipping the input pulses to the 6BN6 grids to 2 x 10^{-9} sec., took the resolving time down by a factor of 2-3, as was expected.

An average of 2 runs using cosmic ray coincidences, again gave effectively the same resolving time. Peaking of the resolution curve over the resolving time, with a much cleaner cutoff, reflects the fact that most of the cosmic coincidences counted were high pulse height events, for which the 6BN6 biases were set appropriately more negative to preclude single pulse triggering. The peaking of the curve then qualitatively demonstrates that the individual pulses are thin, and well separated at peak over the coincidence counting interval. Graph VI-6, Appendix E, is a plot of the 2 run average, normalized, counting rate vs delay.

One run was made using actual Co^{60} coincidences, which corroborated the previous results of about 3 x 10^{-8} sec.

Several runs were made using real coincidences from events produced in a target in the Synchrotron beam. No attempt was made to identify the coincidence particles, nor was differential energy discrimination attempted. The results indicated a resolving time of about 3 x 10^{-8} sec. As was expected, the observed resolving time decreased markedly as

6BN6 biases were made more negative. In effect, by the change in biases, we selected out of the spectrum of pulse heights, the higher pulse heights for which the results of the measurement are explained as for the cosmic ray curve peaking. Graphs VI-8 are the plot of these data.

In the mu pair experiment the pulses into each grid circuit will be random in pulse height, and single grid discrimination will be of no use.[25] It is proposed then, to use the 6BN6 as a crude discriminator by keeping both grids at the same value of bias. Table 6-3 shows representative values of discriminator voltage versus equal grid-bias settings.

---

25 Practicability of the use of the 6BN6 as a dual discriminator is questionable in view of the number of parameters involved. The grids are not symmetric with respect to their behavior at identical grid voltages, because the limiter grid is so much closer to the cathode than is the quadrature grid. Plateau-break curves were plotted for various input pulse heights as a function of the two variables; quadrature grid voltage and limiter grid voltage; (Graphs VI-9, Appendix E.) For a fixed value of limiter grid voltage (-3^v), the plateau-break curves show a very clean cut-off of counting rate as quadrature grid bias is increased. To use the circuit as a discriminator, it is necessary to run at input voltages lower than about 5 volts, i.e., in the region where a small change in input voltage requires a large change in discriminator voltage. For instance, at a quadrature bias of -4.5 volts, a change of bias of 1/2 volt discriminates between pulses differing by only 1/4 of a volt. At pulse inputs above 5 volts, however, discrimination becomes very poor.

Table 6-3

For equal bias settings, the voltage at the input that is discriminated against. Data is for a reduction in counting rate by $\left(1-\frac{1}{e}\right)$.

BIASES	VOLTS INPUT	BIASES	VOLTS INPUT
3x3	1.2	6x6	4
4x4	1.9	7x7	10
5x5	2.4		

The table shows discrimination for input pulses of equal height. For the random pulses we shall be using in the experiment, then, these values will be only approximate.

Some tentative energy discrimination tests were made with a Co^{60} γ source (1.16, 1.32 Mev) - producing real coincidences in test scintillation detectors. Cut-off was very broad and poorly defined in this test.

A survey of the tests of the 402 amplifier--6BN6 coincidence circuit indicates that, for purposes of this experiment, certain basic criteria should be met:

1. Operate the 6BN6 at biases between -3 volts and -6 volts to minimize spurious effects due to secondary pulses and overshoots and to keep the tube in an operating condition (i.e., Where the average pulse height expected can cause coincidence).
2. Operate the 402 amplifiers at high gain (each stage at -1.5 volts bias). The voltage from the output-dynode is of the order

of .1 to .3 volts, for which we can expect 4 stage gain up to the saturation level of the amplifiers. The number of observable noise pulses from the tube (5819) is increased thereby, but because of the fast resolving time of the circuit, no significant increase in normal accidentals' rates results.

3. Use the 6BN6 as a crude discriminator only, because of the random pulse heights which it will have to accept. Testing will be done in the beam for the correct biases to cut out much of the background of events that lose less than 2 Mev.

4. Operate the rig at the peak of the coincidence resolution curve by using the appropriate cable lengths.

B. Final Electronics System

A block diagram of the electronics circuitry and components for the final experiment is shown in Figure 6-3.

Dependent on the factors discussed in Chapters III, IV, and V, and within the limitations thereby imposed, a mu pair entering the meson (inner) detectors (M_I and M_{II}) produce a coincidence pulse in the 6BN6 circuit.

The meson-coincidence pulse (M_I-M_{II} coincidence) is presented, through a discriminator-amplifier, and a Model 501 amplifier, to the timing circuit as the timing initiator. The timing sequence begins with a fixed 1/2 or 1/4 microsecond delay, followed by the 6 microsecond electron gate pulses, a separate gate for each detector system I and II.

The decay of each meson produces an electron coincidence pulse in detectors $(E\text{-}M)_I$ and $(E\text{-}M)_{II}$. The (E-M) electron-

FIG. 6-3

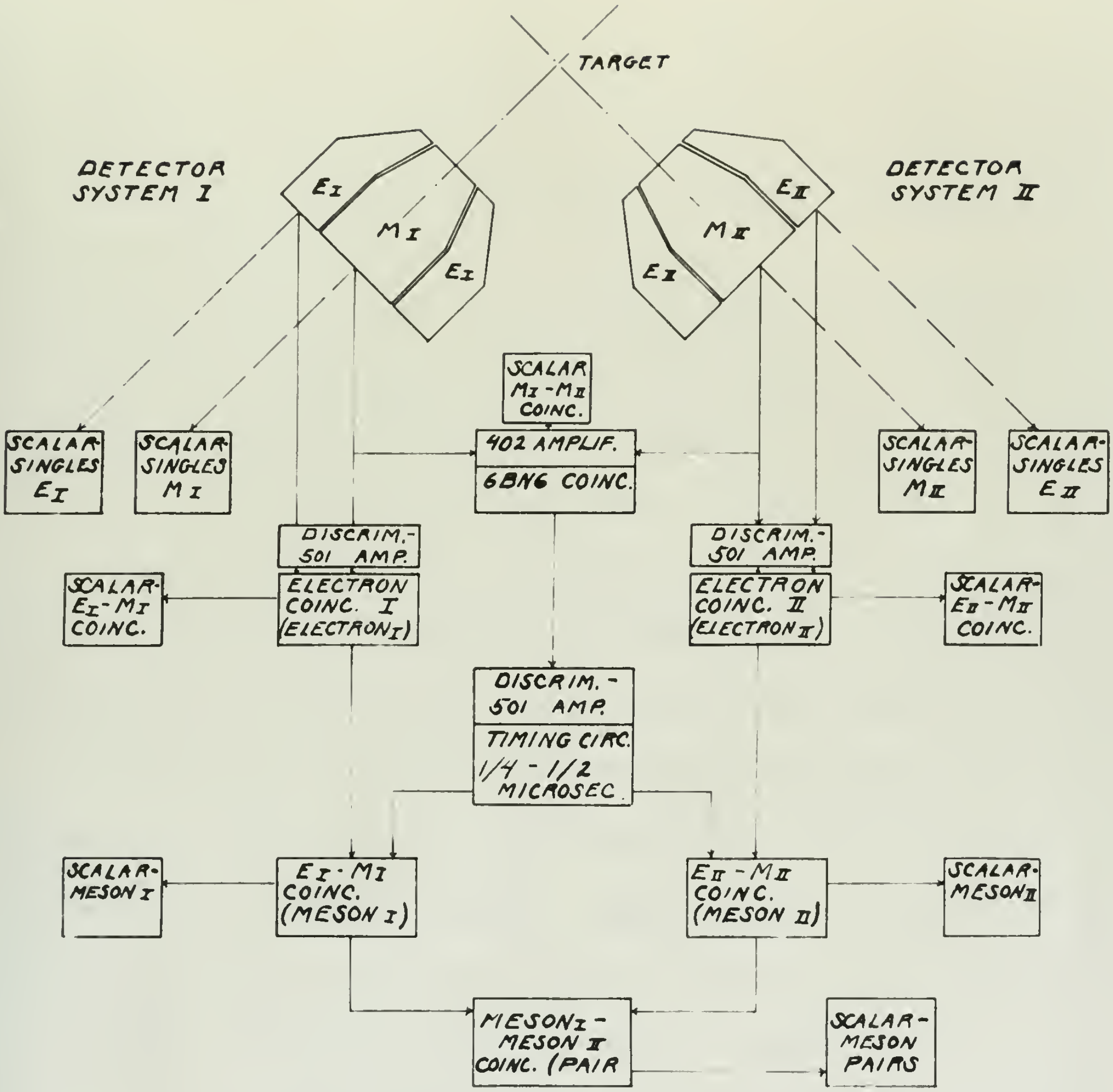

FINAL DESIGN ELECTRONICS FOR MU PAIR DETECTION

coincidence is required to reduce the spurious gate-coincidences which would arise from stray electrons or photons in the B detector, for instance. Note, that although the time to decay of each mu is neither predictable, nor the same for the members of a pair, only a small fraction, $\exp - t/\tau_\mu$, is uncollected in gate length $6\,\mu s$. (modified by the fast decay factor, Chapter IV). So, essentially all the decay electrons are "caught" in the 6 microsecond gate.

The (E-M) electron-coincidence pulse (hereafter the "electron" pulse, E_I or E_{II}) is presented to the 6 microsecond gate of each system, producing the single "pair-electron" coincidence pulse (hereafter called the "meson" pulse, M_I or M_{II}).

The meson pulses, M_I and M_{II}, from systems I and II are required to be in coincidence in a slow circuit (resolving time 6 microseconds) to form the final counted pair pulse.

Scalars are used to determine the singles rates of detectors M_I, M_{II}, E_I, E_{II}; the "electron" singles rates, $(E-M)_I$ $(E-M)_{II}$, and the "meson" singles rates $Meson_I$ and $Meson_{II}$, in the 6 microsecond gate circuit of each system, and the final meson-pair rate, "$Meson_I$ - $Meson_{II}$."

The emphasis throughout has been to reduce the chance rates to a minimum.

Although the very slow final coincidence circuit has a resolving time of 6 microseconds, the singles rates "$Meson_I$" and "$Meson_{II}$" will be so slow (10^{-3} counts per mouse) even if the 6BN6 M_I - M_{II} coincidence were not required, that it is

believed the meson-pair rate will be pure.

The output connections of the photomultipliers of each detector are connected in parallel: two tube common for the meson (inner) detectors, and four tube common for the electron (outer) detectors. The parallel connection does not increase the single tube output time constant by much, and causes a decrease in pulse height which is acceptable. Two output pulses are taken from the duo: a negative signal from the last dynode to a common lead into a cathode follower stage as one input to the electron coincidence circuit ($Electron_{II}$); a positive signal from the next to last dynode to a common lead as one input to the 6BN6 meson coincidence circuit (M_I-M_{II}). In the quartet a common negative pulse from the last dynode is taken into a cathode follower stage as the second input to the electron coincidence circuit (Electron). The cathode follower circuits for both duo/quartet are identical and are matched to 100 ohm cable at the output (Figure 6-4).[26]

---

[26] Dr. Osborne advised that, in order to reduce parasitic oscillations in the cathode followers, special wiring of the 6J4 socket be made: the extra grid pins, 5 and 6, were clipped short and an electrostatic shielding bar of copper was connected from pin 4 (ground filament) across the center pin, and to chassis ground, separating the plate, pin 7, from the grid, pin 1. In addition a 25 ohm resistor was snubbed to the grid pin, from which resistor the normal grid connections were made.

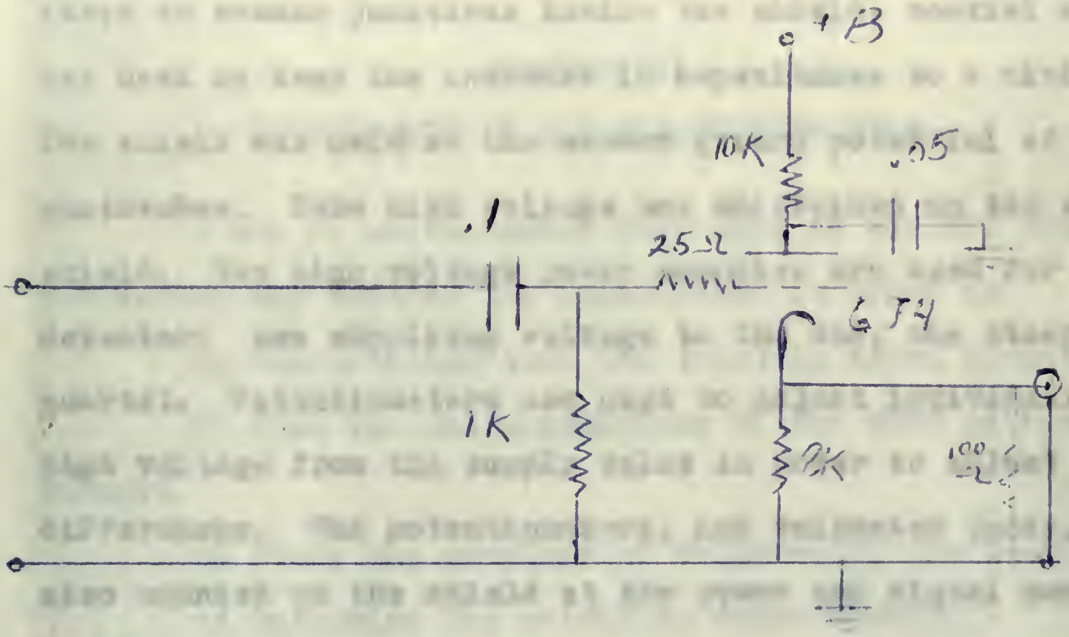

FIG 6-4

As an electrostatic shield and light-tight box, a cylindrical brass frame extends from the rear of each detector system rearward 8", with a detachable cover for the end, through which electrical connections and adjustments are made. The phototube mount, and particularly the "O" ring seal, provides mechanical support for the tube, magnetic shield and tube base extending back from the detector end plates. The cathode follower circuits are mounted on the inside of the shield wall. All power and signal connections are through light-tight fittings on the outside of the shield cylindrical wall. Where it was necessary to run signal leads from individual

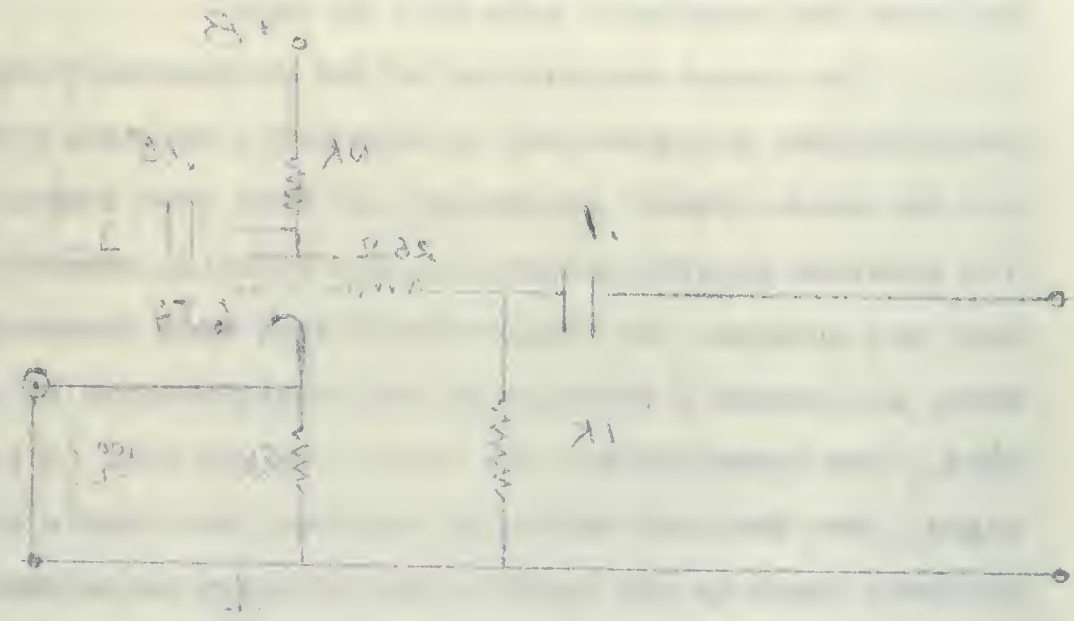

tubes to common junctions inside the shield, coaxial cable was used to keep the increase in capacitance to a minimum. The shield was held at the common ground potential of all the phototubes. Tube high voltage was maintained on the magnetic shield. Two high voltage power supplies are used for each detector: one supplying voltage to the duo, the other to the quartet. Potentiometers are used to adjust individual tube high voltage from the supply value in order to adjust for tube differences. The potentiometers, and voltmeter jacks, are also mounted on the shield at the power and signal connection point.

CHAPTER VII

EXPERIMENTS IN THE SYNCHROTRON BEAM

A set of measurements were made in the 320 Mev bremsstrahlung beam of the Synchrotron in order to:

1) Evaluate and test the existing meson electronics.

2) Test the characteristics of the 6BN6 coincidence circuit.

3) Study the problems of collimating the beam.

4) Determine the shielding requirements.

5) Minimize the background, and ascertain that no background was being overlooked.

6) Determine the feasible upper limit of the length of run, to set a lower limit on the pair production cross section.

In the first experiment, with the geometry shown in Figure 7-1, the first two of the above items were studied.

The 6BN6 circuit was used for coincidence between two detectors in line, a two inch cyclohexylbenzene-5819 detector, and the original Clark detector - a two inch xylene-1P21 detector. This coincidence pulse was taken through a discriminator-amplifier, a model 501 amplifier, and into the timing circuit to commence the timing sequence. Electron pulses, formed by an inside-outside coincidence in the Clark detector, were presented to the timing gates via discriminator-amplifier, and model 501 amplifier. In this particular phase

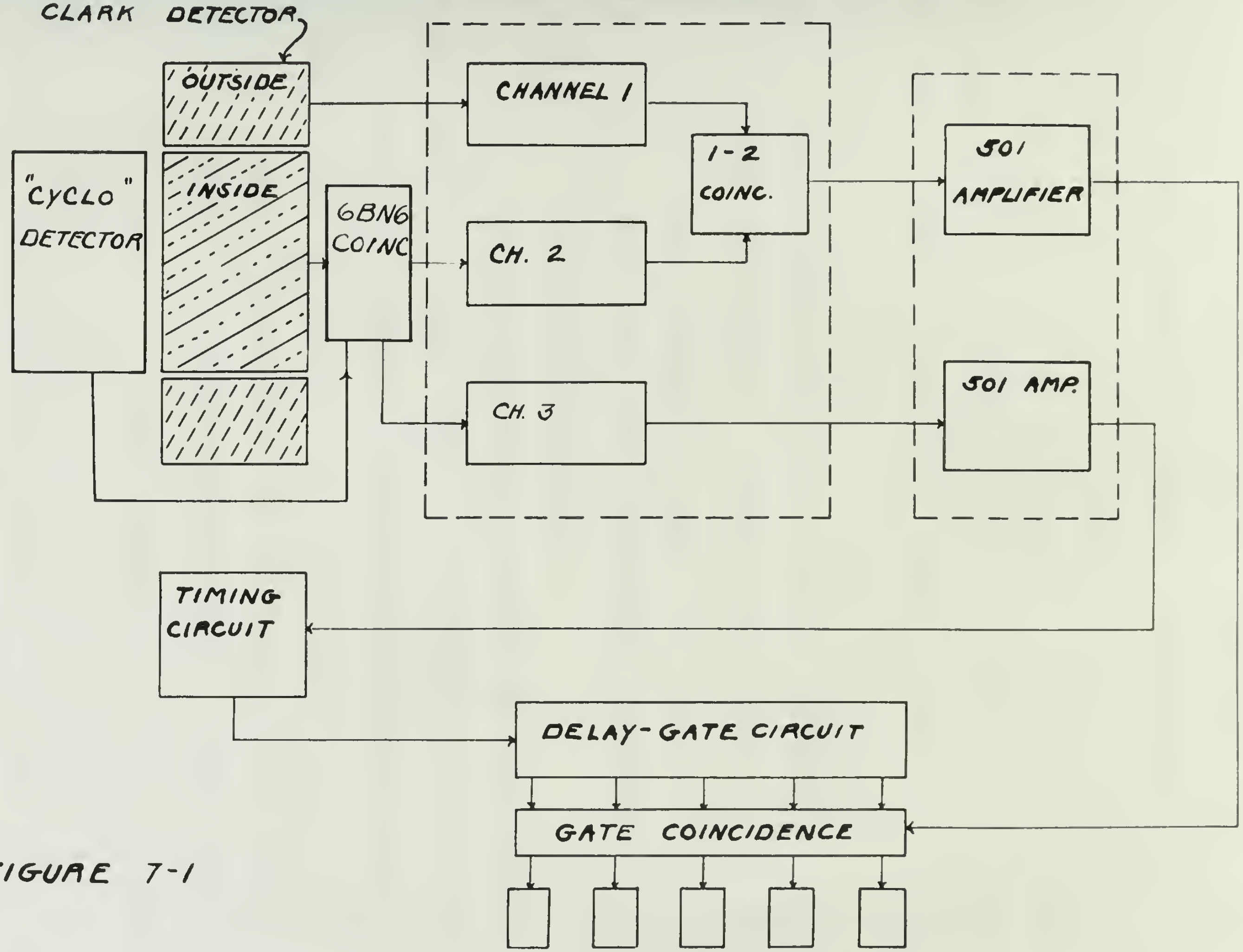

FIGURE 7-1

SCHEMATIC DIAGRAM OF CIRCUITRY FOR INITIAL TEST OF MESON ELECTRONICS WITH ORIGINAL CONCENTRIC DETECTOR.

the electronics were used as designed, i.e. with the timing sequence signal beginning after a fixed delay of 1/2 microsecond. A series of four contiguous 1 1/2 microsecond gate pulses and a 6 microsecond accidentals' gate, followed the 1 1/2 microsecond delay. Each gate coincidence circuit drove a scalar.

The average of 6 runs at 105° is shown in Graph VII-1, the decay time characteristic of photomesons produced in CH_2. The 6BN6 was found to perform as anticipated from the studies with cosmic rays and other tests (q.v. Chapter VI). The pulses from the 6BN6 were quite readily adapted to triggering the meson electronics. Checks were made on the possibility that the 6BN6 was failing to register all true coincidences. The investigation showed that negligible losses, if any, were occurring in the 6BN6 electronics.

As a second experiment a series of geometries similar to that shown in Figure 7-2 were employed to study items 3 and 4 of the list above. The detectors were placed at various distances from the target; runs were made with and without target; various arrangements of collimation were employed; varying amounts of shielding were placed around the detectors.

The results of these studies led to the design geometry shown in Figure 3, Appendix A. Extreme collimation was found desirable. The scattering of electrons in the beam is a source of many singles counts in the detectors, and it may be desirable to try to clean up the beam magnetically. The most serious demands on shielding exist on the side of the

FIG. 7-2

PAIR GEOMETRY FOR PRELIMINARY EXPERIMENTAL RUNS

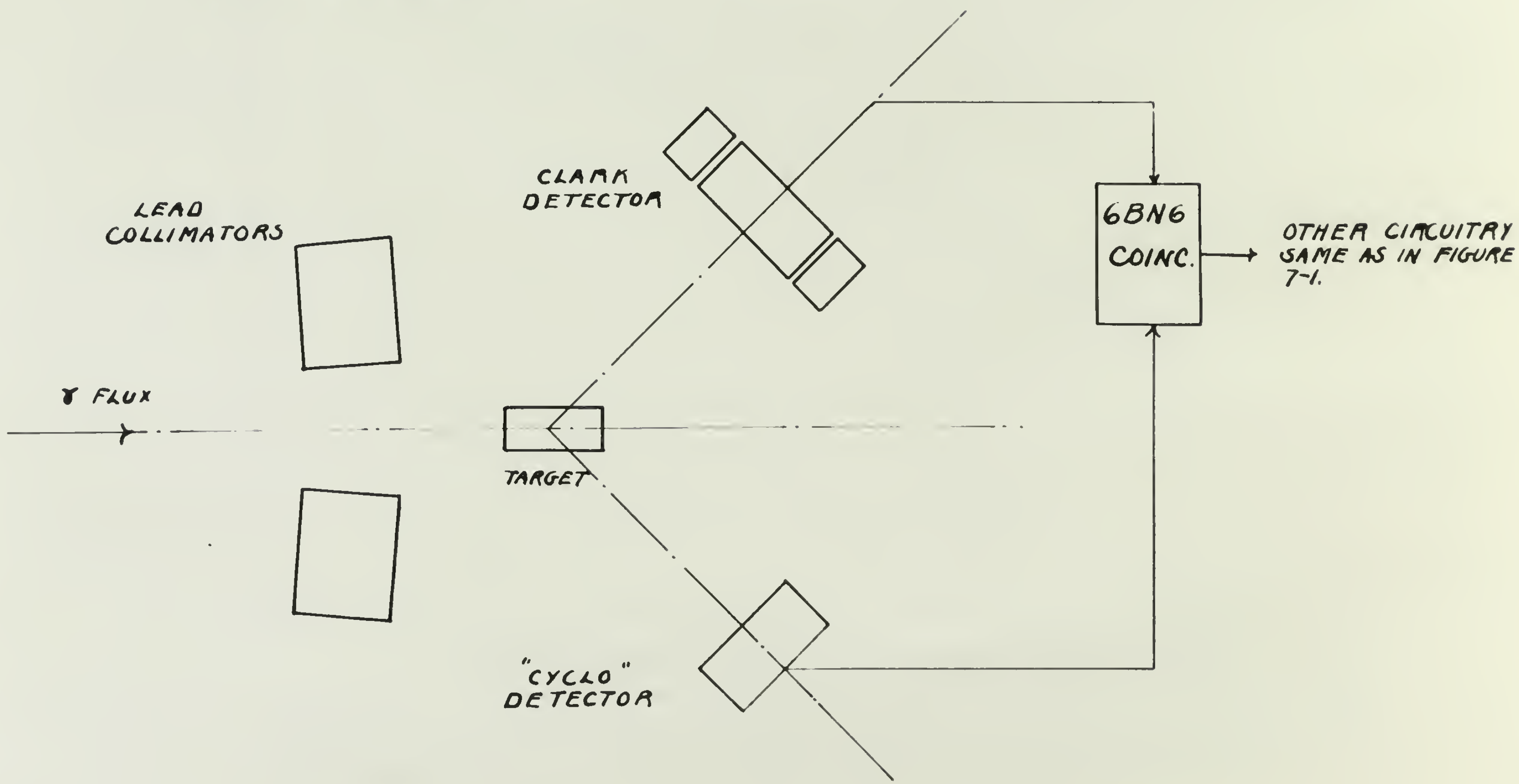

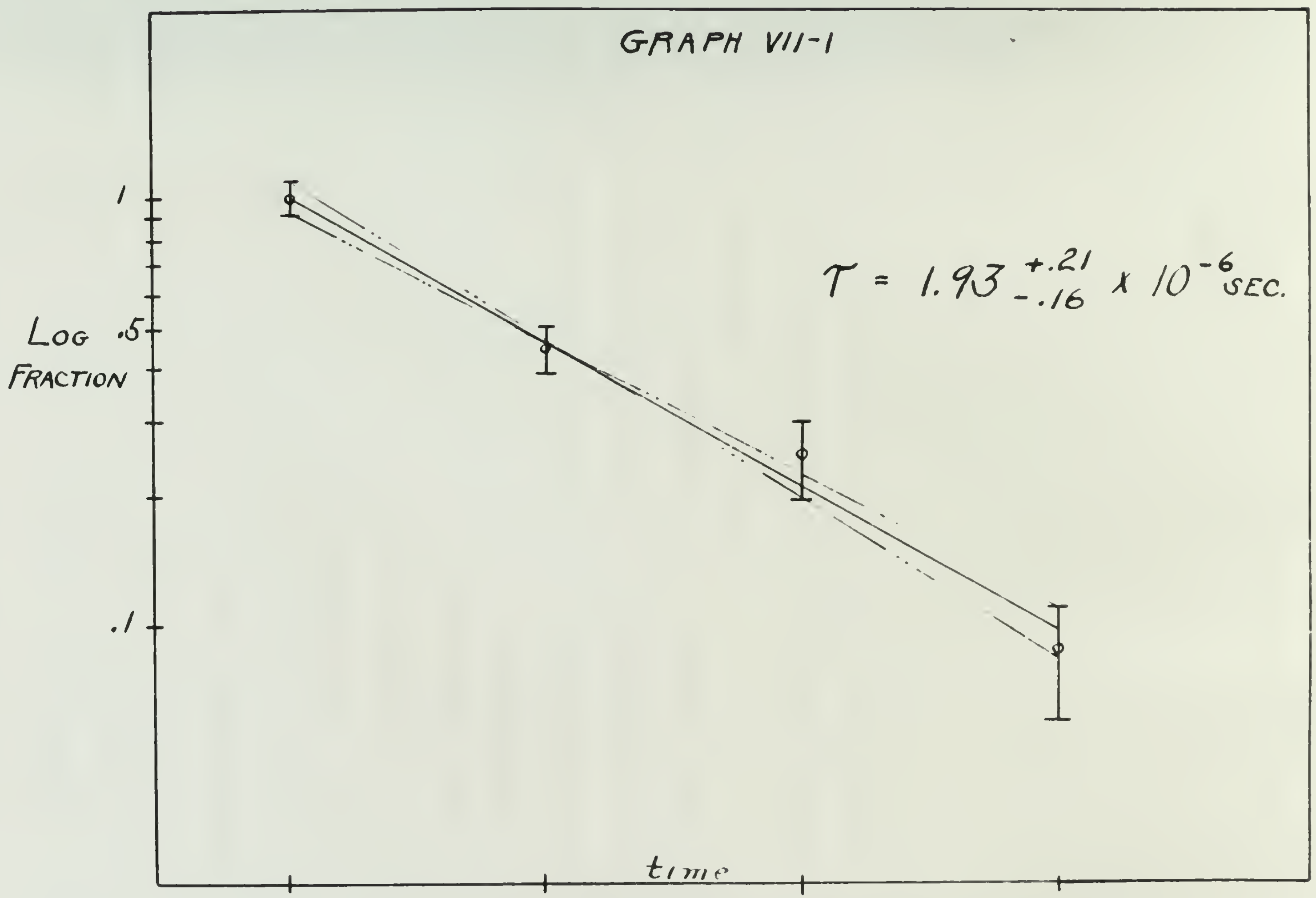

PHOTOMESON PRODUCTION FROM CH_2 AT 105°.
EXPONENTIAL DECAY OF MU MESONS DETECTED IN CONCENTRIC GEOMETRY DETECTORS THROUGH 1½ μsec DELAY GATE - AVERAGE OF FIVE (5) RUNS. LOG (FRACTION IN GATE) vs. GATE DELAY IN MICROSECONDS.

housing facing the target.

In a third series of measurements, items 5 and 6 of the above list were studied with the geometry shown in Figure 7-2. The Clark detector was used for system I, the cyclohexylbenzene-filled detector, alone, for system II. The electronics remained the same as for the phase I and II runs: i.e. a coincidence was required in the 6BN6 circuit between the "cyclo" detector and the inner Clark detector as before.

It was found that unless at least 1/4 inch of lead was placed in front of the detectors, the soft radiation created in the target (or scattered by the target) made the singles counting rates too high.

Using 3 inches of lead in front of the detectors established that neutrons were an insignificant background. All studies led to the conclusion that electrons, positrons, and γ rays were the greatest source of background counts at 45°. There were no indications of unanticipated backgrounds.

From Figure 7-2, it can be seen that the detection efficiency for mu pairs was extremely low. Because of the short length of each meson detector (2 inches), we were restricted to those pairs that shared the available energy equally, plus or minus a few Mev. The fraction of the total pairs rejected is therefore very considerable, at least .9 for the 320 Mev photons, and more for the lower energy events. Also the effective solid angle factor is very small.

Taking 12 inches and 14 inches as the effective

detector distances, and noting that the Clark detector was collimated to three inches, the cyclohexylbenzene detector to four inches, the factors of equation IV-1b, for the detection efficiency become approximately:

$$\mathcal{E}_c = 2\,\Delta\omega_1 \Delta\omega_2 \cdot \delta^2 \cdot x \cdot \eta^2 \cdot g \cdot f$$

$$\mathcal{E}_c = (3.92\times10^{-3})(5.1\times10^{-3})(.62)(1)(.03)(.05)(4)(2)$$

so that the approximate efficiency for these runs was:

$$\mathcal{E}_c = .16 \times 10^{-6}$$

The runs with this space separated geometry, although made under adverse conditions,[27] established some interesting facts:

1. The Y coincidence rate (6BN6 coincidence between the meson detectors on either side of the target) was established as composed of one-third real events, and two-thirds accidentals. This was determined by delaying one of the pulses sufficiently to throw it out of the resolving time bracket of the other pulse by factors of 4 to 4.5.

2. The electron-coincidence rate (inside-outside coincidences in the Clark detector) was comprised of two-thirds to three-fourths real events, independent of what shielding we did, and at this large target distance.

For a particular run of about 10^{11} quanta--2500 "ratz"--with a thin (two inch long) Be target, and 1/4 inch

---

[27] The "set-up" was made downstream from another experiment which was being conducted concurrently with this one.

lead absorber, the following results were obtained:

Meson-pair accidentals rate[28].....0004 per "ratz" = .000274 per mouse (or 4×10^{-12} per e.q.)

Meson-pair rate, 3 sec gate......0008 per "ratz"

Meson-pair rate, 4.5 sec gate....0004 per "ratz"

We are in a position to set an upper limit on the Wentzelian process from the above run. For the calculation, we assume we would have been able to identify a real rate that was equal to the accidental rate, 2.74×10^{-4} per mouse.

For the two inch Be target, the effective target length (equations V-4 and V-5) is 4.77 cm, and the e.q. per mouse, corrected for actual target area, is equal to α' of Equation V-6, 4.46×10^{7} e.q. per mouse.

The expected yield (equation V-7) is:

$$Y = .16 \times 10^{-6} \times 1.23 \times 10^{23} \times 4.46 \times 10^{7} \times 4.77\ I$$

$$Y = .437 \times 10^{25}\ I$$

or $2.74 \times 10^{-4} = .437 \times 10^{25}\ I$

and $I = .627 \times 10^{-28}$

where $I = \int \sigma(E)\, d(\ln E)$

Assuming σ constant, $I = \sigma \ln E \Big]_{215}^{320}$, hence,

$$I = .4\sigma = 6.27 \times 10^{-29}$$

$$\text{or } \sigma \approx 1.57 \times 10^{-28}\ cm^2$$

which is about 2.5×10^{5} times the electromagnetic process cross section, essentially the same limit established by

---

[28] It is felt that when two mu-meson delayed coincidences are put into coincidence, the above accidentals counting rate should decrease by at least a factor of 10^2. If this conservative estimate is correct, one would get 1 event in about 10^5 mice. This is the basis for the estimate made in Chapter V of the number of mice per run.

Martinelli.[29]

As is remarked in Chapter V, the electromagnetic process, or the Wentzelian process with an integrated cross section of 10^{-33} cm^2, have a marginal detection probability with the MIT machine. It is interesting to note that if a factor of only 10 could be gained by a combination of increase in beam intensity and Bremmstrahlung energy, observation could probably decide whether the process is occurring or not. As a matter of fact, the detection efficiency may be increased almost this much over the minimum figure used for the yield calculations, from the Z dependence, and $\Delta\omega$ correlation effects mentioned in Chapter IV. If this be so, experimental runs in the MIT beam should be able to establish the process, if it does occur.

If counting rates are obtained near the predicted values for the electromagnetic process, some method of separating the relative contribution of the electromagnetic and Wentzelian modes to the rate will have to be established. It is possible that such a determination will have to await the building of machines of much higher energies and intensities.

The author is very deeply indebted to Dr. Wattenberg and Dr. Feld for their active guidance, unceasing interest, and generous assistance in this work. Dr. L. S. Osborne, whose meson electronics were used in the preliminary experiments,

---

[29] Ibid.

was unfailingly generous with his time and help. Mr. Carmen Pupi of the MIT Machine Shop skillfully constructed the detectors.

Many thanks are also due others of the Synchrotron Laboratory in particular: A. Odian, P. Stein, P. Zlochiver, D. Gagliardi, J. Rosengren, and G. Pugh for their timely and succinct assistance.

BIBLIOGRAPHY

BIBLIOGRAPHY

Bell, Hincks,: PR., 84, 1243 (1951).

Conversi, Pancini, and Piccioni; PR. 68, 232 (1945); PR. 71, 209 (1947).

Dirac, P.A.M., Principles of Quantum Theory.

Fermi, E., Nuclear Physics; Notes compiled by Orear, Rosenfeld, and Schulter.

Gingrich, N.S., Rev. Mod. Phys. 15, 19 (1943).

Heitler, W., Quantum Theory of Radiation.

Hough, P.V.C., PR. 73, 1 February 1948.

Hubbard, H.W., Thesis, University of California, 10 March 1952, "Positron spectrum from decay of mu mesons."

Marshak, R.E., Meson Physics.

Mather, Martinelli, and Jarmie, UCRL 1166 W 7405-eng-48, University of California.

Pauli, V., Weisskopf, V.F., Helv. Phys. Acta., 7,7,709 (1934).

Peterson, Gilbert, White, PR. 81, 1011 (1951).

Rossi, Nereson, PR. 62, 417 (1942).

Seitz, Mueller, PR. 78, 605 (1950).

Sigurgeirrson, T, Yamakawa, K.A., Rev. Mod. Phys., 21, 124, 1949.

Thorndike, A.M., Mesons - a summary of experimental facts.

Ticho, H.K., PR. 74, 1337 (1948).

Wentzel, H.K., PR. 79, 710 (1950).

APPENDIX

APPENDIX A

DETAILS OF DETECTOR CONSTRUCTION

CYCLOHEXYLBENZENE SEALS:

The sealing gaskets were hand cut from a laboratory plastic, the name of which remained unknown after exhaustive inquiry. The material is a pliant sheet, 1/8 inch thick, with the interesting and useful properties of insolubility in cyclohexylbenzene, but very good solubility in water.

The gaskets were hand cut because of the difficulty of jigging for a lathe operation, and trouble with "chattering" tools, which produced ragged, and off-size pieces.

Ductility of the plastic is fairly good, but it possesses a very low compressibility, so that the 1/16 inch throw for sealing pressure was more than adequate. (The gasket grooves were milled to 1/16 inch in the back plates.)

ALUMINUM REFLECTOR LINING:

The interior bodies of both inner and outer detectors were fully lined with 2 mil Aluminum foil. The foil was bonded to the brass with ARALDITE Compound, No. XV, a resin manufactured by the CIBA Co. of New York City.

The detectors were made up in preliminary form in four sections:

Piece 1. Outer wall and target end piece of outer detector.

Piece 2. Inner wall and back plate of outer detector.

Piece 3. Cylincrical walls and target window of inner detector.

Piece 4. Back plate of inner detector.

The four pieces were completely seamed and soldered at their respective joints as for finished junctions. A study of the description of the four pieces will show that all interior surfaces are accessible for applying the reflector. Further, each piece was strengthened by the joints, so that the heat necessary to cure the ARALDITE did not warp them.

Prior to aluminizing, the pertinent surfaces were washed down with HNO_3 in solution, followed by water rinses and washing with alcohol to clean and degrease the surface for the resin.

The pieces were heated to 135° C in a temperature regulated oven, then the ARALDITE, in stick form, was applied by rubbing off a thin melt on the hot metal surface. The Aluminum was placed on the metal-melt surface and lightly rolled with a cylindrical glass tube to remove creases and bubbles as much as possible. The resin bonds were then cured for 12 hours at 125° C.

Chemical solubility of the ARALDITE in cyclohexylbenzene is not known, but several samples were tested for apparent solubility by immersion in the scintillator liquid.

The cured ARALDITE exhibited no effects whatsoever,

while the raw resin showed a tendency toward slight "wetting" after 5 days immersion. Similar "wetting" occurred in water. No evidence of solubility was seen. After 3 weeks of immersion, the cured ARALDITE appeared untouched by the liquid, which showed no discoloration or other physical signs of solution.

CYCLOHEXYLBENZENE

The liquid was obtained commercially from the MONSANTO CHEMICAL COMPANY Factory in St. Louis, but it was not known whether in pure form or not.

Purification was accomplished by successive filterations through 25 inches of Activated Alumina (ALCOA), Mesh 28-48, and 3 inches of glass wool.

FIGURE 1, APP. B

DETECTOR

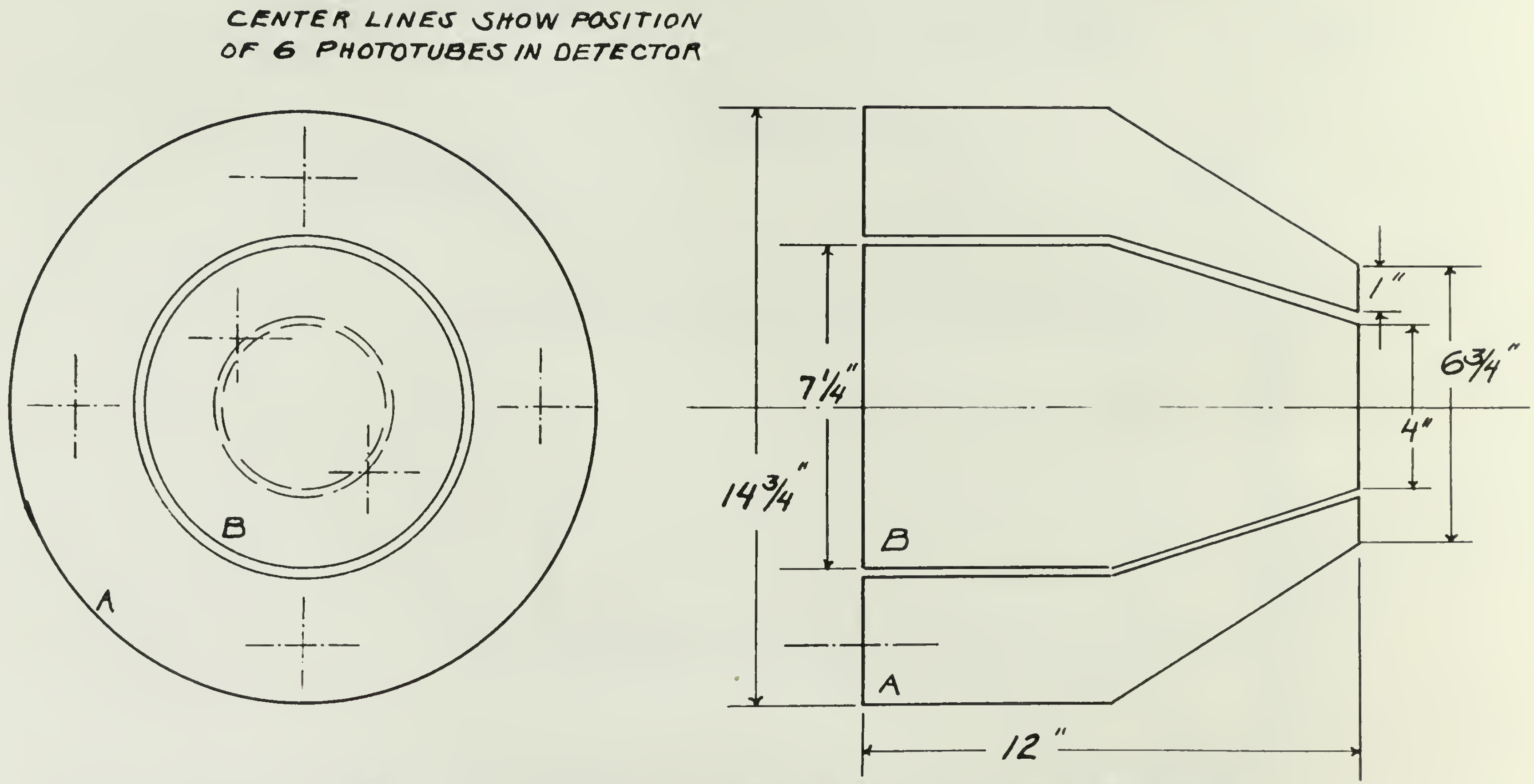

NEW DESIGN CONCENTRIC SCINTILLATION DETECTORS. CYCLOHEXYLBENZENE FILLED WITH P-TERPHENYL SOLUTE. OUTER WALLS OF DETECTOR "A" ARE 1/16" SOFT BRASS. INNER WALLS OF "A", WALLS AND WINDOW OF DETECTOR "B" ARE .020" BRASS. BACK PLATES ARE 3/16 INCH BRASS TO PROVIDE STRONG TUBE MOUNTING. FOR DETAILS OF PHOTOTUBE MOUNTING SEE FIGURE

DETAILS OF PLASTIC
PHOTOTUBE MOUNT

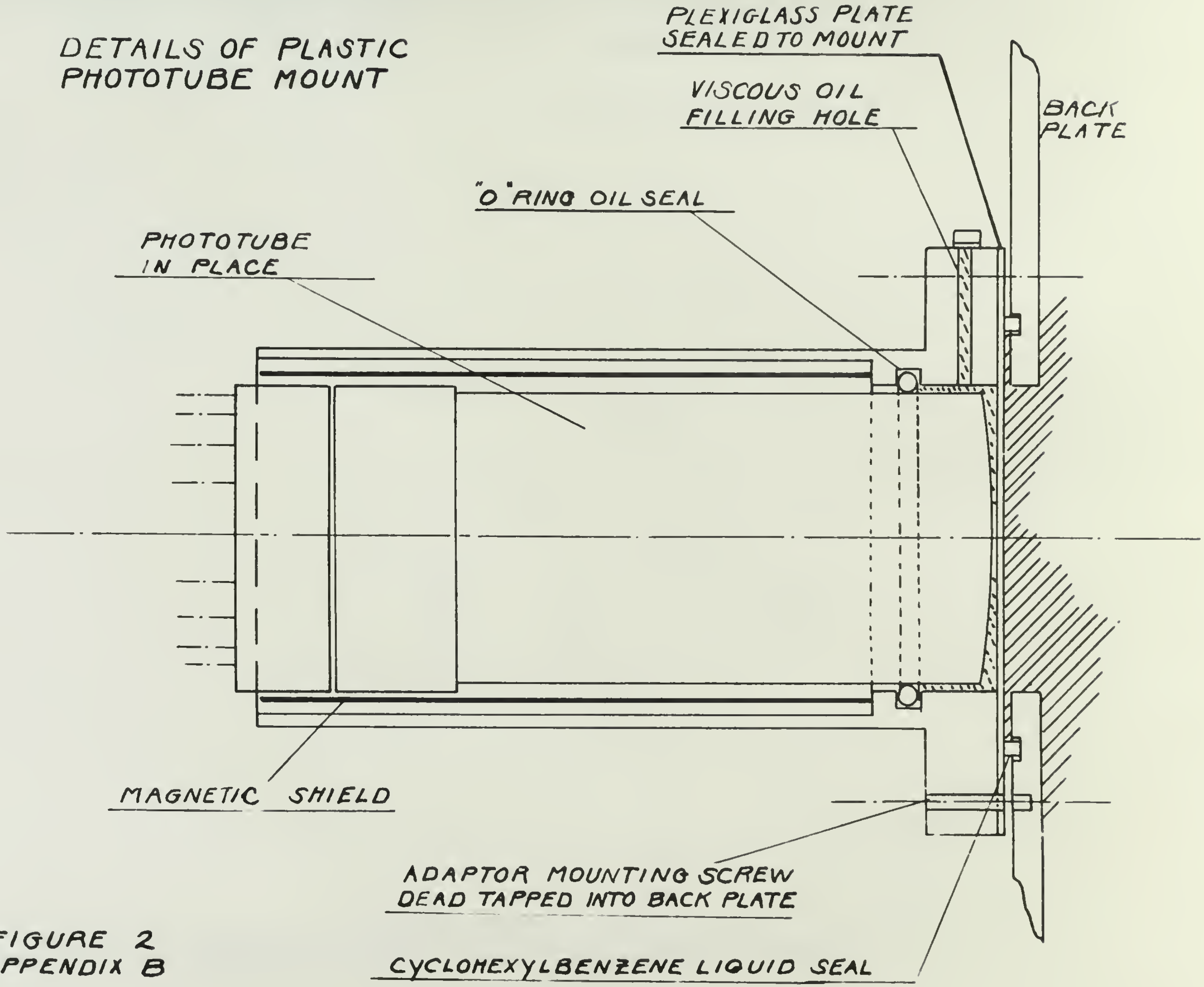

FIGURE 2
APPENDIX B

FIGURE 3, APP B

EXPERIMENTAL GEOMETRY
MU MESON PAIR DETECTION

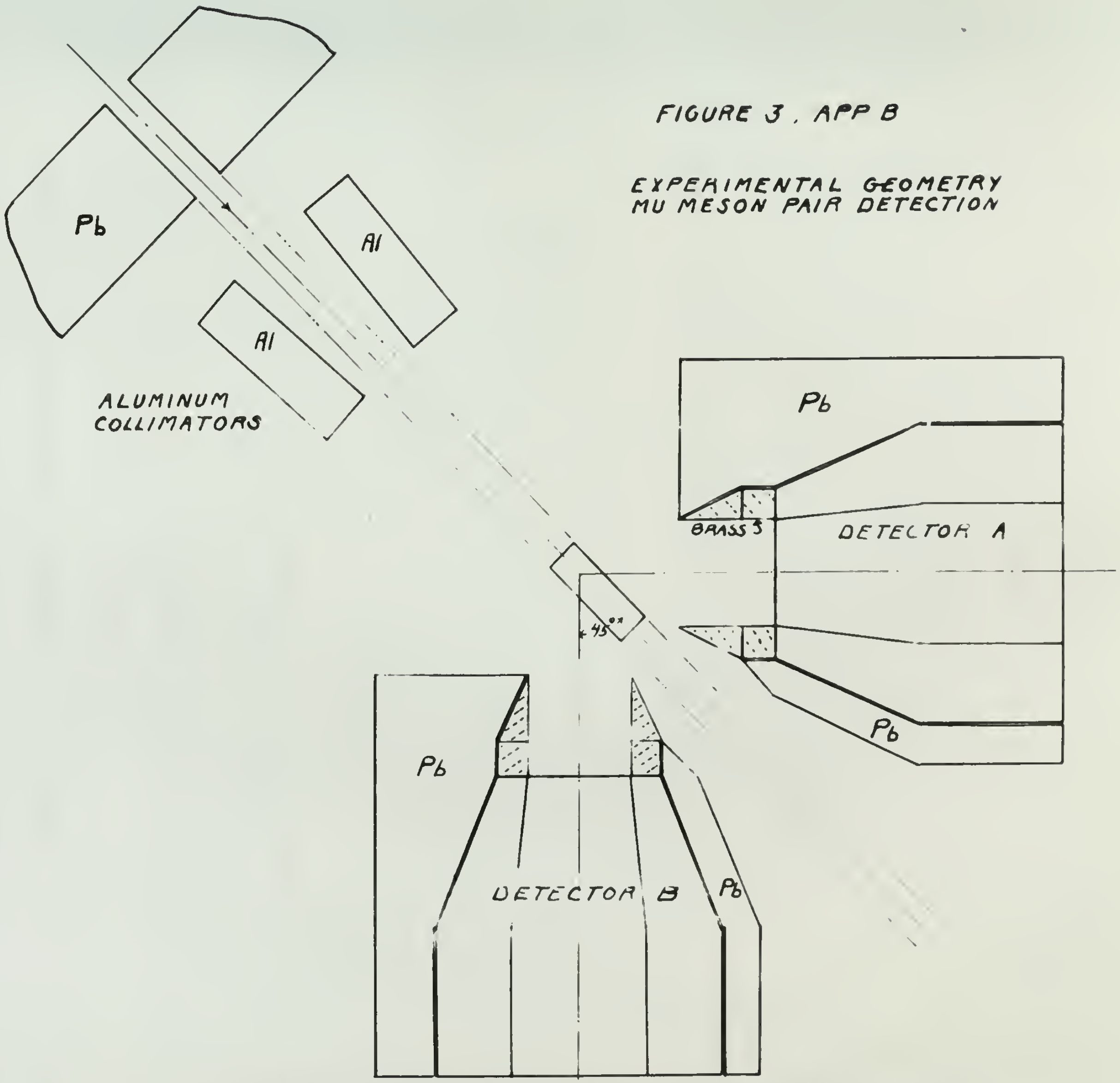

DETECTION GEOMETRY WITH SPECIAL CONCENTRIC DETECTORS
SYNCHROTRON BEAM COLLIMATED TO ONE INCH WIDTH

APPENDIX B

ORDER OF MAGNITUDE ESTIMATE OF THE NUMBER OF EFFECTIVE PHOTONS AT THE PHOTO-CATHODE, PER MEV LOST

This calculation is carried out for the outer detector of each system (the electron detector) which has a total photo-cathode surface of four 5819 tubes (8 square inches). The walls of the detector are lined with reflecting foil.

Consider Figure B-1, a section in a plane containing the axis of symmetry of the detector system. Photons produced at P have a random distribution in direction. Because of the toroidal geometry of the actual detector, the calculation is probably not completely accurate, but since most of the peripheral reflections will be at large angles, it is felt that the results will be highly indicative.

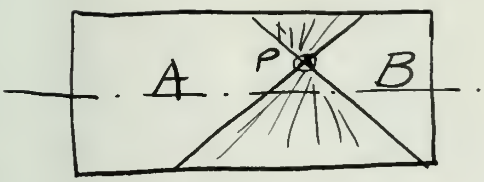

FIG B-1

Let us assume that the photons emitted in solid angles A and B above, are in the acceptance cone, and that they comprise about 1/3 of the total solid angle.

Then, taking the reflection coefficient for the aluminum reflector as .8,[30] the fraction of the photons collected after

---

[30] Most handbooks give for the reflectivity about .9. We take .8 to account for the creases and folds in the reflector which produce non-predictable reflection directions.

reflections, is, for cone B: $1/6\,[\,.8\,\frac{a}{A} + (.8)^3\frac{a}{A} + (.8)^5\frac{a}{A} + \ldots\ldots]$

where a is the total area of the four photocathodes and A is the area of the back walls into which the phototubes are inset.

The factor $(.8)^n$ is the diminution of intensity of the photon group for n reflections. (The energy loss, for 3 ev photons, is due to absorption at reflection only.)

The fraction collected from cone A is:

$$1/6\,[\quad 1 \times \frac{a}{A} + (.8)^2\frac{a}{A} + (.8)^4\frac{a}{A} + \ldots\ldots]$$

The total fraction collected from cone A and B is:

$$f = 1/6 \sum_{n}^{\infty} (.8)^n \frac{a}{A} = 1/6\,\frac{a}{A}\left(\frac{1}{1-.8}\right) = \frac{5}{6}\,\frac{a}{A}$$

$a = 4 \times \pi$ cm^2, the area of 4 photocathodes

$A = \pi \times (9.4^2 - 6.4^2)$ cm^2, the area of the back face, for a toroidal cyclinder of 3 inch radial thickness.

$$\frac{a}{A} = \frac{4 \times \pi}{\pi(9.4^2-6.4^2)} = \frac{4}{88-41} = \frac{4}{47} = .085$$

$$f = 5/6\,\frac{a}{A} = 5/6(.085) = .0709$$

Now let us reduce this by a factor of 2 to take account of the circumferential reflection possibilities, such that:

$$f' = \frac{.0709}{2} = .0355$$

We take the scintillator conversion efficiency as about

.005, for converting energy to light; and the photocathode efficiency as about 1/10, for the fraction of incident photons that produce secondary electrons at the cathode.

Now, per Mev of energy loss, the expected number of 3 ev quanta produced with conversion efficiency of .005 is:

$$\varphi = \frac{10^6 \times .005}{3} = 1667$$

The number collected in the gross cathode area per Mev is then:

$$N = f' \times \varphi = .0355 \times 1667 = 60$$

Whence, applying the photo-cathode efficiency of 1/10 gives, for the number of secondaries produced per Mev lost:

$$N_e = 60 \times 1/10 = 6 \pm 2 \text{ per Mev.}$$

APPENDIX C

APPROXIMATE CALCULATION FOR EFFICIENCY FACTOR η

Consider an infinitely-long cyclindrical meson detector, surrounded by a hollow toroidal cylinder for electron detection.[31]

We assume Hubbard's spectrum.[32]

The criteria for exit of the decay electron will be simply the decay energy and the relative position in the detector at decay.

The approximate calculation is made for the special case of center line decay, for a detector of average radius, 2.5 inches. The density of the cyclohexylbenzene is taken as .8 gms per cm^3, i.e. the average radial thickness denoted below by "a" is 2.5 x 2.54 x .8 = 5.8 gms.

The electron spectrum for the decay is taken from Hubbard:

$$f(E)dE = dE \frac{12E^2}{W^4} [(W-E) + 2/9 \rho (4E-3W)] \qquad \text{C-1}$$

where ρ is "...a parameter determined by the amounts of the various interactions causing mu meson decay." Hubbard's

---

[31] A correction must be made to the calculation with the infinite cylinder for the loss of decay electrons in the solid angle subtended by the front face--wherein there is no outer detector volume. We will take .8 of the result as an estimate for this end effect.

[32] _Ibid_.

results show good agreement with theory for ρ = .26.

We take ρ here to be = .25, and combine the bracket to:

$(W-E) + 2/9(.25)(4E-3W) = (W-E) + .22E-.17W$

or $(.83W-.78E) \cong .8\ (W-E)$

or $f(E)dE = dE\ 9.6/W^4\ E^2\ (W-E)$ C-2

where $W = \frac{m_\mu c^2}{2} = 55$ Mev.

The number in energy interval dE at E is f(E). The calculation assumes emission from the decay position in a random direction.

The direction of emission for a given energy determines how far the electron will travel before stopping. Assuming that the minimum ionization loss of 2 Mev per gm. occurs throughout the transit, the direction of emission relative to the axis uniquely determines whether or not the decay electron can exit the center detector. Consider Figure C-1.

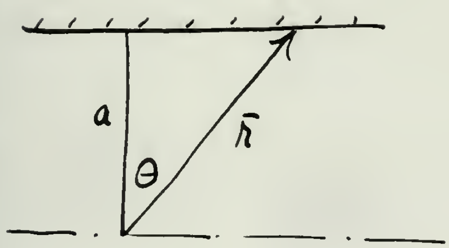

FIG C-1

$\bar{r}$ is the direction of emission.

a is the average radial thickness in gms.

Then the electron loses:

$g'(r) = 2 \times r$ Mev in exiting (r in gms) C-3

Allowing 4 Mev excess for loss in a double wall thickness, an ionization in the outer detector, a detectable electron must have energy:

$$g(r) = (2 \times r + 4) \text{ Mev}$$

$$\text{or} \quad g(\Theta) = \left(2 \frac{a}{\cos} + 4\right) \text{ Mev} \qquad \text{C-4}$$

$$\text{Let } U = \int dV \int_{g(\Theta)}^{W} f(E)\, dE$$

where U is the "useful" energy of the spectrum for detection of the decay electron, as a function of the lower limit $g(\Theta)$.

The fraction of the spectrum energy available as "useful" energy is:

$$\frac{U}{U_o} = \frac{\int dV \int_g^W f(E)\,dE}{\int dV \int_0^W f(E)\,dE} = \frac{\int d\Theta \sin\Theta \int_g^W E^2(W-E)\,dE}{\int d\Theta \sin\Theta \int_0^W E^2(W-E)\,dE} \qquad \text{C-5}$$

The integral $\int E^2(W-E)\,dE = \left(\frac{E^3 W}{3} - \frac{E^4}{4}\right)$

$$\text{whereupon: } \frac{U}{U_o} = \frac{\int \sin\Theta \, d\Theta \left[\frac{W^4}{12} - \left\{\frac{g^3 W}{3} - \frac{g^4}{4}\right\}\right]}{\int \sin\Theta \, d\Theta \left(\frac{W^4}{12}\right)} \qquad \text{C-6}$$

$$\text{or, } \frac{U}{U_o} = \frac{\int_0^\pi \sin\Theta \, d\Theta \left[1 - \left\{\frac{4}{W^3} g^3 - \frac{3}{W^4} g^4\right\}\right]}{\int_0^\pi \sin\Theta \, d\Theta} \qquad \text{C-7}$$

$$\text{or, } \frac{U}{U_o} = 1 - \frac{\int_0^{\Theta} \sin\Theta \, d\Theta \left\{\frac{4}{W^3} g^3 - \frac{3}{W^4} g^4\right\}}{\int_0^\pi \sin\Theta \, d\Theta} \qquad \text{C-8}$$

where the upper limit of the volume integration of the

numerator is taken as Θ, the limiting angle of emission, for which an electron with the maximum spectrum energy could escape, i.e.: $g(\Theta) = \frac{2a}{\cos\Theta} + 4 = 55$ Mev

$$\cos\Theta = 2a/51 = .227$$

$$\Theta \approx 77^{0} \qquad \text{C-9}$$

Now $$g(\theta)^3 = \frac{8a^3}{\cos^3\theta} + \frac{32a^2}{\cos^2\theta} + \frac{64a}{\cos\theta} + 64 \qquad \text{C-10}$$

and $$g(\theta)^4 = \frac{16a^4}{\cos^4\theta} + \frac{64a^3}{\cos^3\theta} + \frac{192a^2}{\cos^2\theta} + \frac{256a}{\cos\theta} + 256 \qquad \text{C-11}$$

whereupon combining the bracket, $\sin\theta\left\{\frac{4}{W^3}g^3 - \frac{3}{W^4}g^4\right\}$

we have: $$\int_0^{\Theta} d\theta\left\{-\frac{48a^4}{W^4}\left(\frac{\sin\theta}{\cos^4\theta}\right) + \left(\frac{32a^3}{W^3} - \frac{192a^3}{W^4}\right)\frac{\sin\theta}{\cos^3\theta} + \left(\frac{128a^2}{W^3} - \frac{576a^2}{W^4}\right)\frac{\sin\theta}{\cos^2\theta} + \left(\frac{256a}{W^3} - \frac{768a}{W^4}\right)\frac{\sin\theta}{\cos\theta} - \frac{768}{W^4}\right\} \qquad \text{C-12}$$

The integral $$\int\frac{\sin\theta}{\cos^n\theta} \rightarrow \frac{\sec^{n-1}\theta}{n-1} \qquad \text{C-13}$$

So the integrals reduce to: $$\frac{8}{W^3}\left\{-\frac{6a^4}{3W}\sec^3\theta + \left(4 - \frac{24}{W}\right)\frac{a^3}{2}\sec^2\theta + \left(16 - \frac{72}{W}\right)a^2\sec\theta + \left(32 - \frac{96}{W}\right)a\ln\sec\theta - \frac{96}{W}\right\}\Bigg|_0^{\Theta} \qquad \text{C-14}$$

$\sec\Theta = 4.4$ $\qquad \sec^2\Theta = 19.3$ $\qquad \sec^3\Theta = 85$

$\sec 0 = 1$ $\qquad \sec^2 0 = 1$ $\qquad \sec^3 0 = 1$

which leads to the following value for equation C-14:

$$\frac{8 \times (5656)}{W^3} = .272$$

So that, $$\frac{U}{U_0} = 1 - .136 = .864 \qquad \text{C-15}$$

An estimate must now be made of the way in which this

figure is decreased by reason of non-centerline decay. Suppose that the decay electron were mono-energetic, having just enough energy to produce a pulse in the outer detector, if it has decayed on the centerline and been emitted normal to the detector axis. A curve like Figure C-2 would represent the fraction of these normal-incidence, mono-energetic electrons that produce a pulse, as a function of the radial distance from the center line at decay.[33] Of course the decay electrons do not all come off normally, nor from center line. For a cyclohexylbenzene-filled cylinder of 3 inches radius, a relativistic electron will lose on the order of 12 Mev existing normally from the centerline. Integration of equation C-2 shows that less than 1% of the total number of decay electrons have less kinetic energy than 12 Mev.

Figure C-2

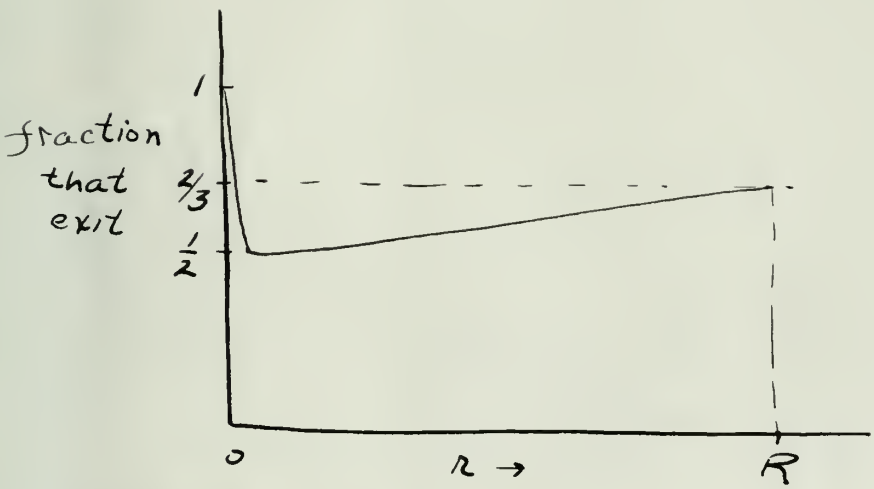

[33]The qualitative shape of this curve may be seen by considering the problem of two disks of equal area whose centers move, from conjunction, to a distance equal to the radius. The area common to the two disks expressed as a fraction of the area of one, corresponds to our fraction that produce a pulse.

For normal incidence decay, an electron with greater than about 24 Mev will be able to exit the inner detector from any point in it. In other words, if all electrons having greater than 24 Mev kinetic energy are normally incident, they will leave the detector; adding 4 Mev for penetration of the double wall, and energy loss in the outer detector, "normal" electrons having greater than 28 Mev will all be counted. The fraction of the decay electrons having greater than 28 Mev is .673.

The fraction of electrons having less than 16 Mev is about .09 (16 Mev is the energy necessary to just exit normally from the center line with 4 Mev excess).

The energy spectrum then contains three regions of interest for these normal incidence decays:

1. Kinetic energy less than 16 Mev.
2. Kinetic energy between 16 Mev and 28 Mev.
3. Kinetic energy greater than 28 Mev.

In group 1, many decay electrons will not be energetic enough to be counted. Let us take that 1/4 of all the normal decays in group 1 are energetically countable.

The fraction of decay electrons in group 2 that will be counted is certainly greater than .5 (see Figure C-2), and is weighted toward a higher fraction, because of the greater likelihood for higher energies than low, in this range. Let us take that about .8 is the fraction collected from this group.

In group 3, collection of the total group is indicated, at least for normal incidence decay.

The combined collection fraction for normal incidence decay is then about .88 for the total spectrum.

Let us apply this factor to extend the evaluation of U/U_o to a fair approximation for the whole volume.

The factor η then becomes:

$$\eta = .864 \times .88 \times .8 = .609$$

$$\text{and } \eta^2 = .37 \qquad \text{C-16}$$

APPENDIX D

TABLE V-1

The integral I^{*} (Equation V-13) $I^{*} = \frac{I'}{C} = \frac{1}{3}(k-2)^3\left(\frac{2}{k}\right)^3\frac{dk}{k}$

E_{max}	E_{min}	k_{max}	k_{min}	I^{*}	$1.12\ I^{*}$
350	280	3.27	2.62	.0574	.0633
340	280	3.18	2.62	.0467	.0523
330	280	3.09	2.62	.0371	.0416
350	260	3.27	2.45	.0622	.0696
340	260	3.18	2.45	.0514	.0575
330	260	3.09	2.45	.0418	.0469
350	240	3.27	2.24	.065	.0728
340	240	3.18	2.24	.0542	.0607
330	240	3.09	2.24	.0447	.0501

The last column $1.12 \times I^{*}$ reflects the 12% plus correction to I^{*} for the Hough cross section at $k=3$, and is taken as an average correction for the range of k in the integrations.

TABLE V-2

Cross section for the electromagnetic production of mu meson pairs from Hough's formulae, mass extrapolated to this process from electronic mass. Z dependence taken to be linear as a lower limit, i.e., complete incoherence assumed. (Cross section times 10^{33} cm^2.)

Energy of the quantum	350 Mev	340 Mev	330 Mev	280 Mev	260 Mev
Be	7.24	6.33/6.2	4.97	1.63	.687
C	10.88	9.49/9.3	8.17	2.44	1.03
Al	23.5	20.55/21	17.7	5.27	2.23
Cu	52.5	45.8/44.9	39.5	10.9	4.97

The values under the slant sign for 340 Mev are the cross sections as per Bethe-Heitler mass extrapolated, with linear Z dependence.

FIG 1 - APP. E

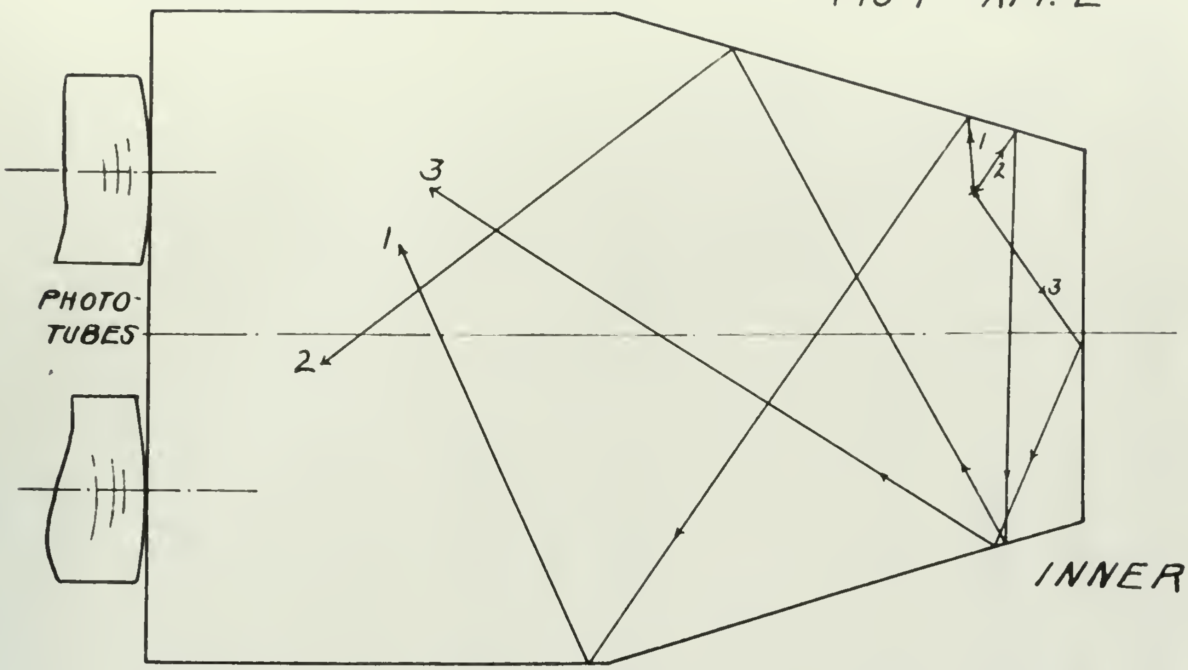

FUNNELLING EFFECT UPON SUCCESSIVE REFLECTIONS IN INNER DETECTOR. THE ILLUSTRATION IS FOR COPLANAR REFLECTION—NOT NECESSARILY TRUE FOR THE DESIGN DETECTORS. THE ROTATION OF REFLECTIONS IN THE CYLINDRICAL GEOMETRY ALTERS THE EFFECT QUANTITATIVELY.

FIG 2 - APP. E

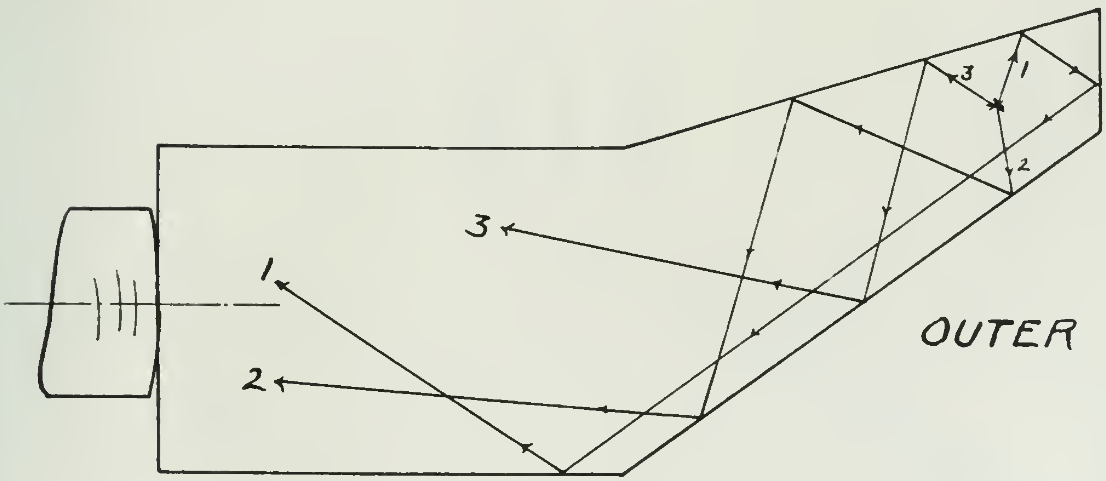

FUNNELING EFFECT UPON SUCCESSIVE REFLECTIONS IN OUTER DETECTOR. SEE REMARKS OF FIG 1 APROPOS NON COPLANAR REFLECTION.

GRAPH IV-1

ENERGY DISTRIBUTION OF PAIRS

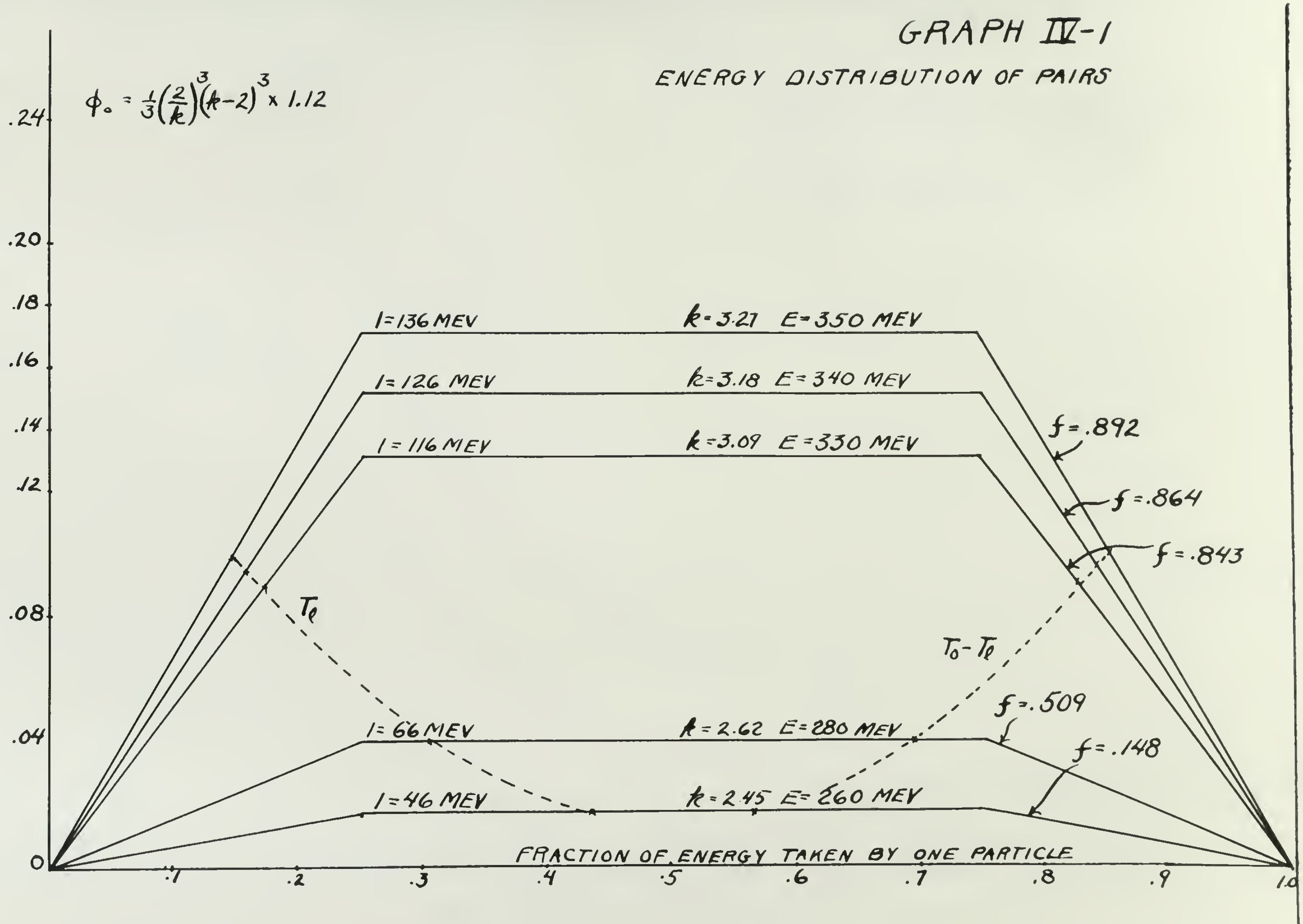

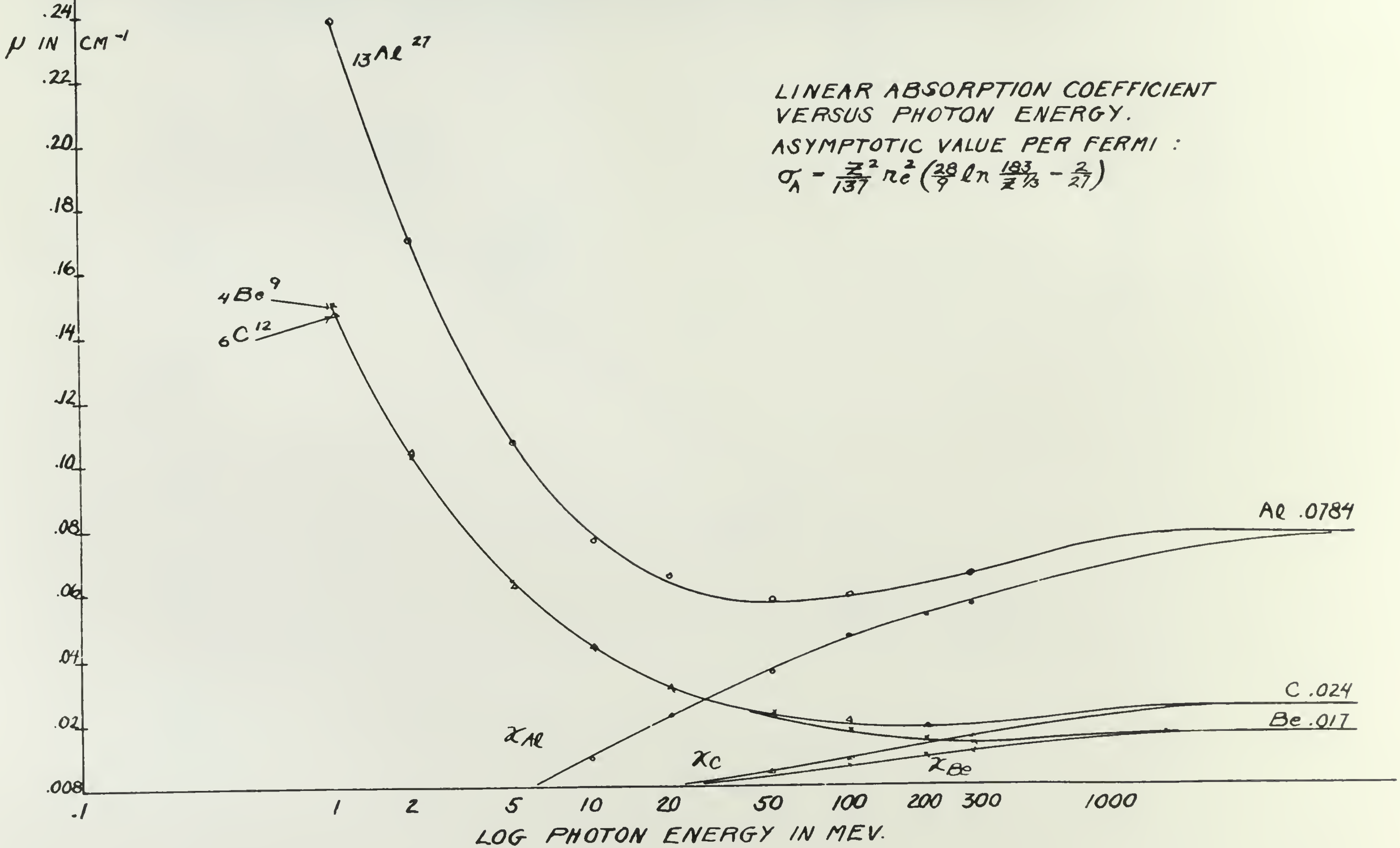
LINEAR ABSORPTION COEFFICIENT
VERSUS PHOTON ENERGY.
ASYMPTOTIC VALUE PER FERMI :
$\sigma_A = \frac{Z^2}{137} r_e^2 \left(\frac{28}{9} \ln \frac{183}{Z^{1/3}} - \frac{2}{27}\right)$
μ IN CM⁻¹
.24
.22
.20
.18
.16
.14
.12
.10
.08
.06
.04
.02
.008
$_{13}Al^{27}$
$_4Be^9$
$_6C^{12}$
Al .0784
C .024
Be .017
χ_{Al}
χ_C
χ_{Be}
.1
1
2
5
10
20
50
100
200
300
1000
LOG PHOTON ENERGY IN MEV.

FIG V-1

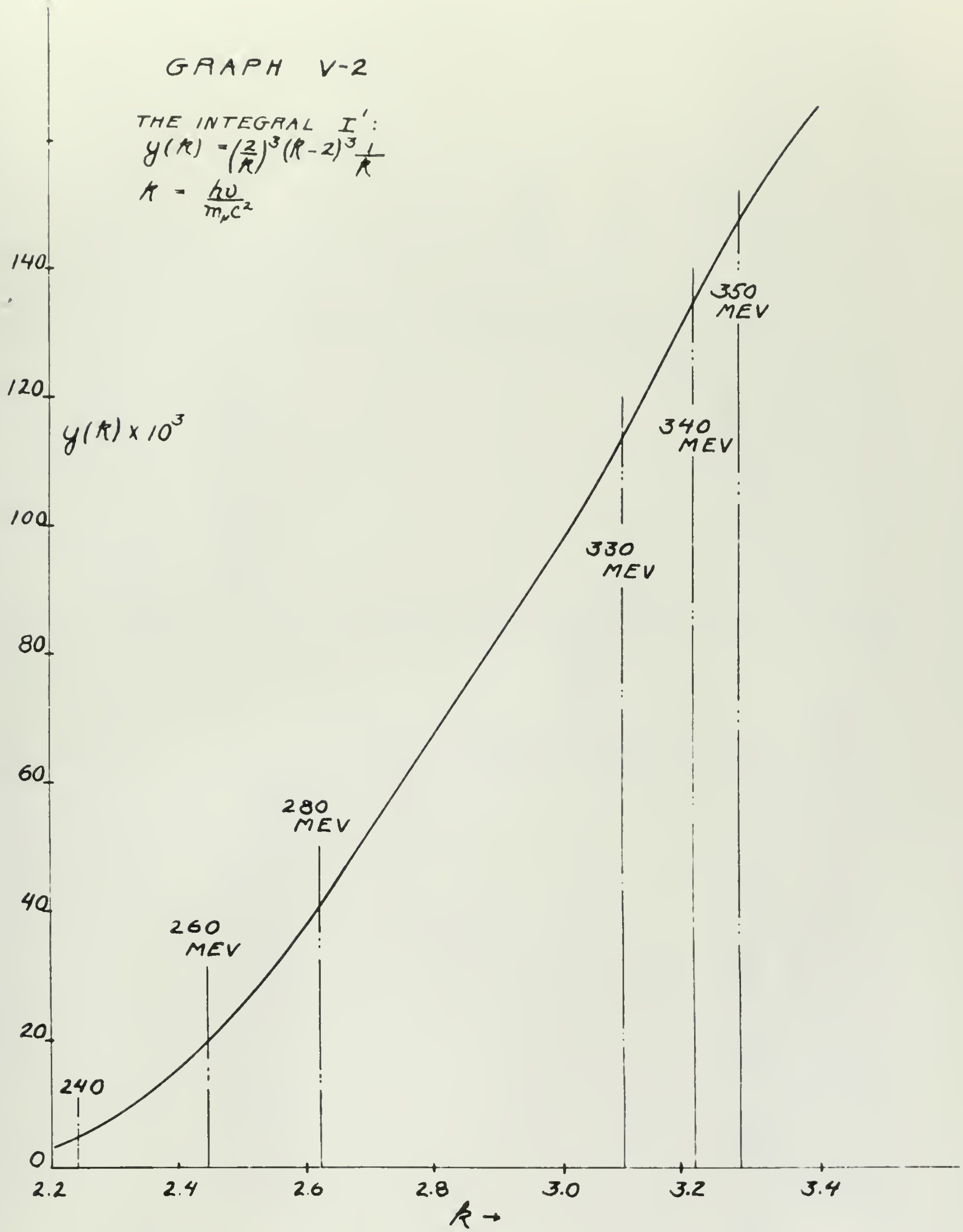

GRAPH V-2
THE INTEGRAL I':
$y(k) = \left(\frac{2}{k}\right)^3 (k-2)^3 \frac{1}{k}$
$k = \frac{h\nu}{m_\mu c^2}$
$y(k) \times 10^3$
0
20
40
60
80
100
120
140
240
260 MEV
280 MEV
330 MEV
340 MEV
350 MEV
2.2
2.4
2.6
2.8
3.0
3.2
3.4
k →

VI-2

6BN6 RESPONSE TESTING --
RISE TIME OF COINCIDENCE PULSE

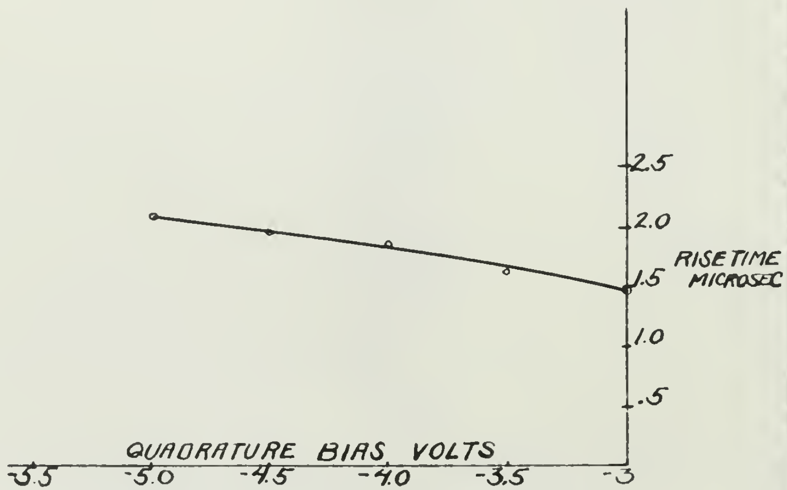

COINCIDENCE PULSE RISE TIME AS A FUNCTION OF QUADRATURE BIAS FOR IDENTICAL PULSE INPUTS ($T_R = 2\mu sec.$) TO BOTH GRIDS - AN AVERAGE FOR LIMITER BIASES FROM -3 TO -5 VOLTS.

VI-1

6BN6 COINC. CIRCUIT
RESPONSE TESTING --
POSITIVE OVERSHOOT

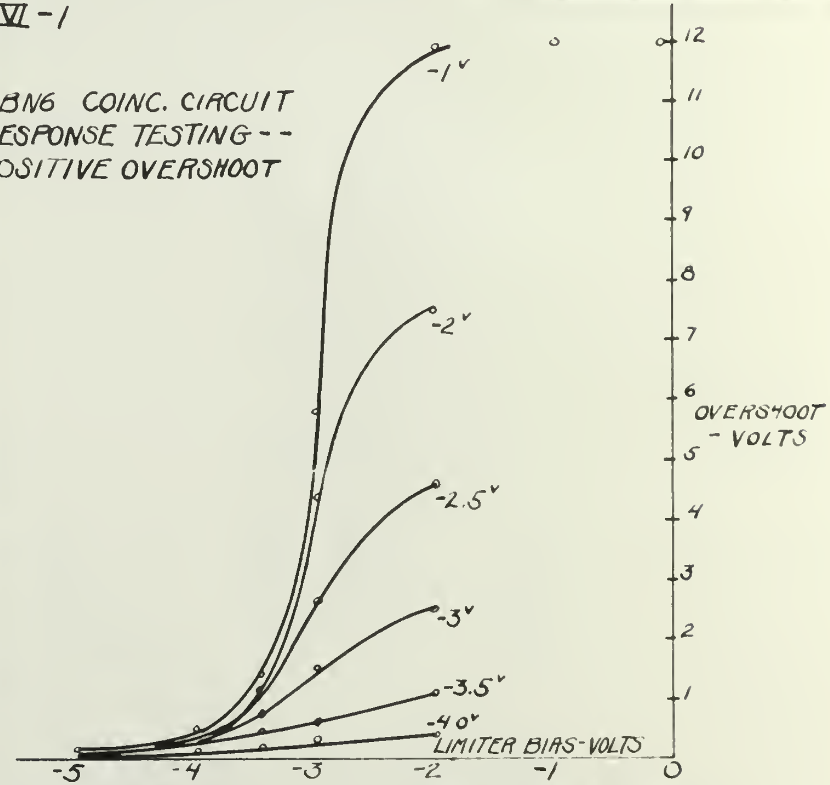

COINCIDENCE PULSE POSITIVE OVERSHOOT AS A FUNCTION OF LIMITER GRID BIAS. IDENTICAL PULSES ($T_R = 2\mu sec$) TO BOTH GRIDS

PARAMETER QUADRATURE BIAS-VOLTS

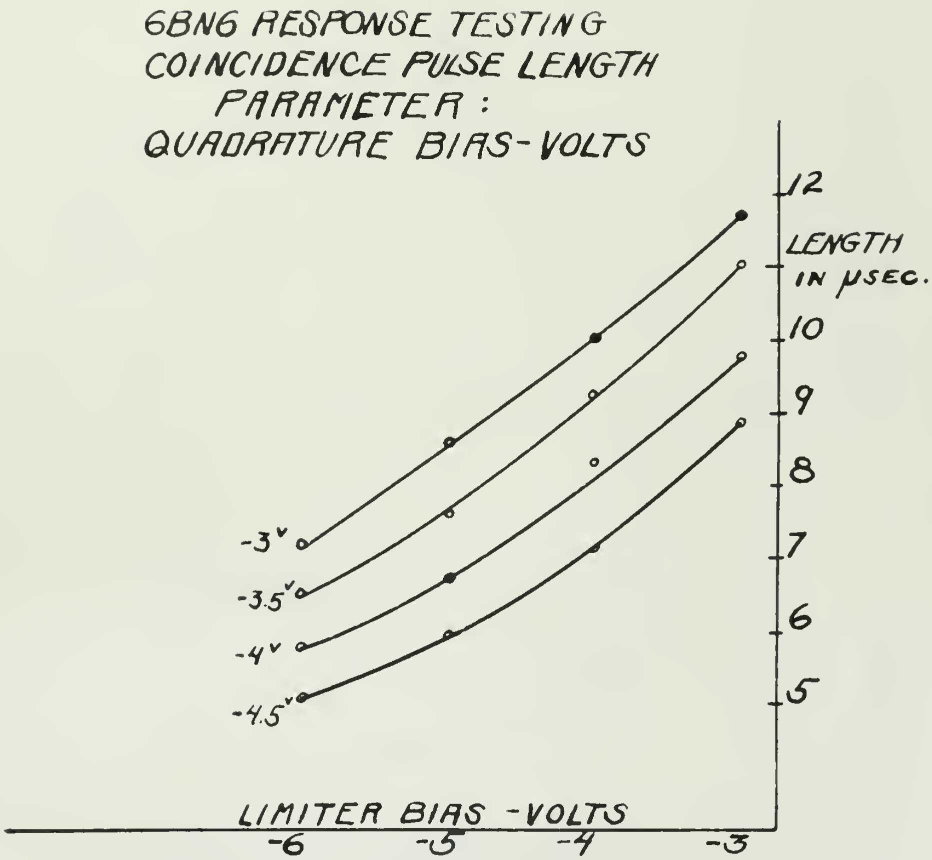

FOR IDENTICAL PULSE INPUTS TO BOTH GRIDS (T_R = 2 μSEC. LENGTH 100 μSEC.)

GRAPH VI-5

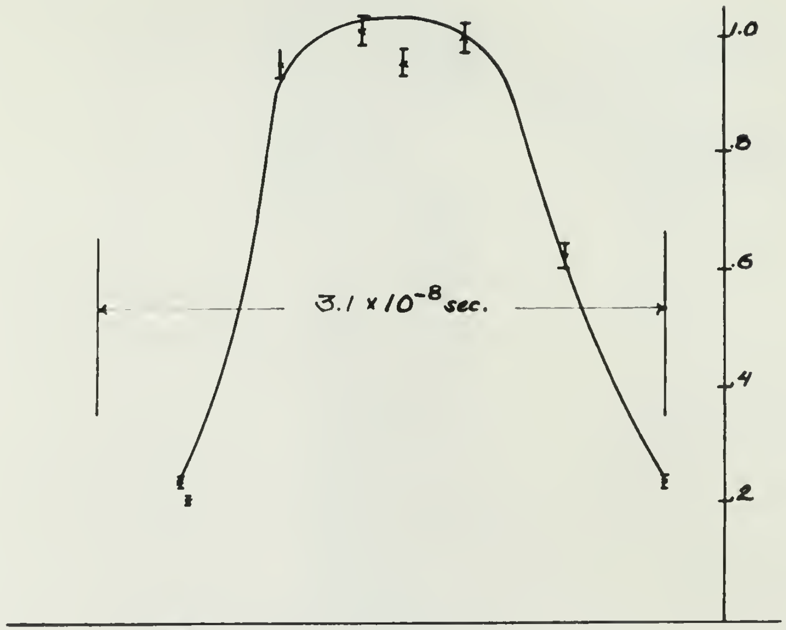

6BN6 RESOLVING TIME
COINCIDENCE COUNTING RATE (FRACTION) AS A FUNCTION OF SIGNAL DELAY.
Ra-γ IN TERPHENYL-CYCLOHEXYLBENZENE.
SPLIT PULSE INPUT.

GRAPH VI-6

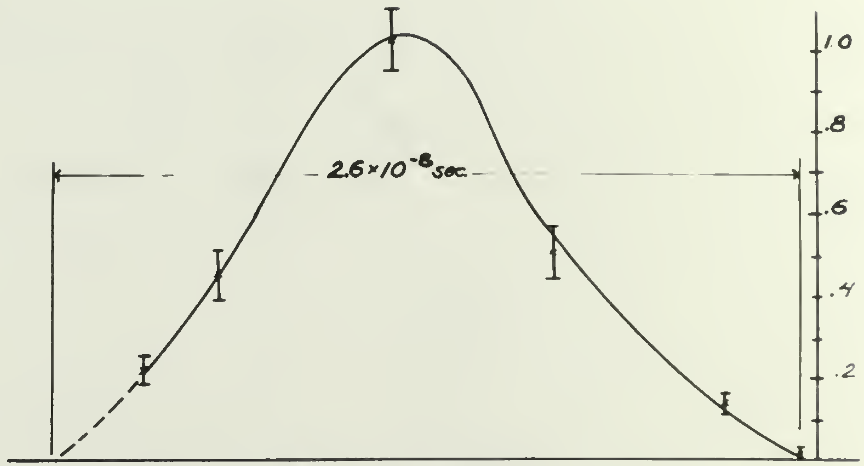

6BN6 RESOLVING TIME
COINCIDENCE COUNTING RATE (FRACTION) AS A FUNCTION OF SIGNAL DELAY.
COSMIC RAY EVENTS IN TERPHENYL-CYCLOHEXYLBENZENE.

GRAPH VI-8

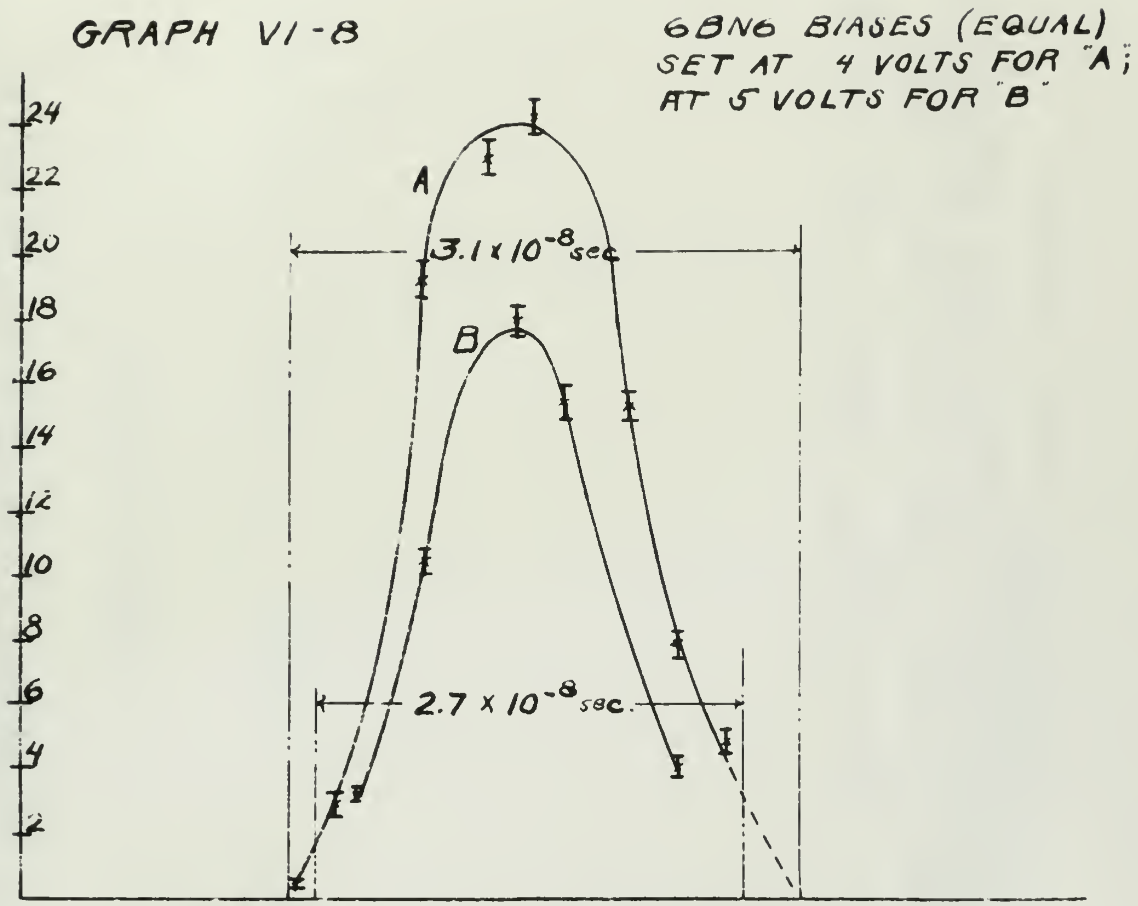

6BN6 RESOLVING TIME

COINCIDENCE RATE "R" (PROPORTIONAL TO RATE PER EQUIVALENT QUANTA) VS SIGNAL DELAY USING COINCIDENCE GEOMETRY DETECTORS COUNTING REAL COINCIDENCES FROM A CARBON TARGET IN THE SYNCHROTRON BEAM.

GRAPH VI-9a

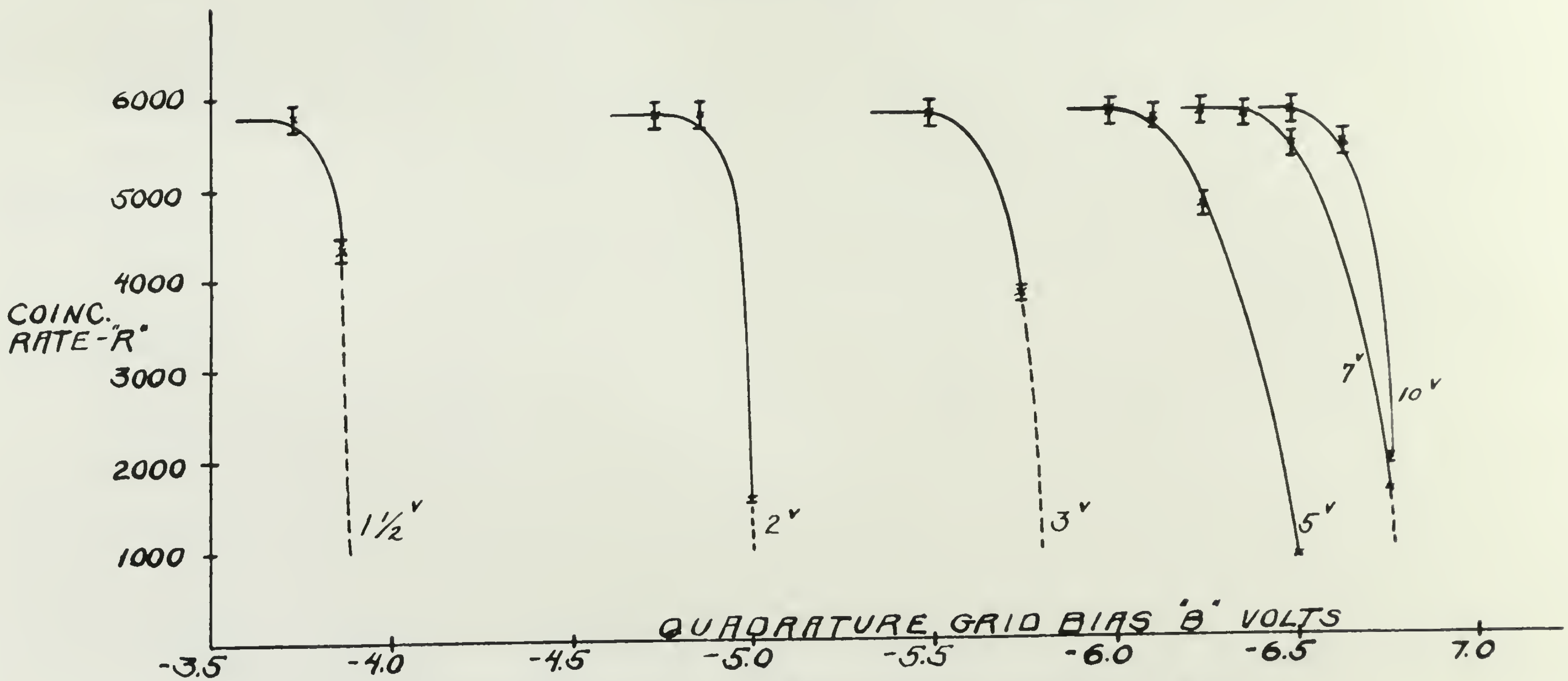

DISCRIMINATOR TESTING - 6BN6 COINCIDENCE CIRCUIT.
COINCIDENCE COUNTING RATE - "R" AS A FUNCTION OF QUADRATURE GRID BIAS - "B."
PARAMETER - INPUT PULSE HEIGHT IN VOLTS - EQUAL PULSE HEIGHTS ON BOTH LIMITER AND QUADRATURE GRIDS.
LIMITER GRID BIAS -3 VOLTS

GRAPH VI-9b

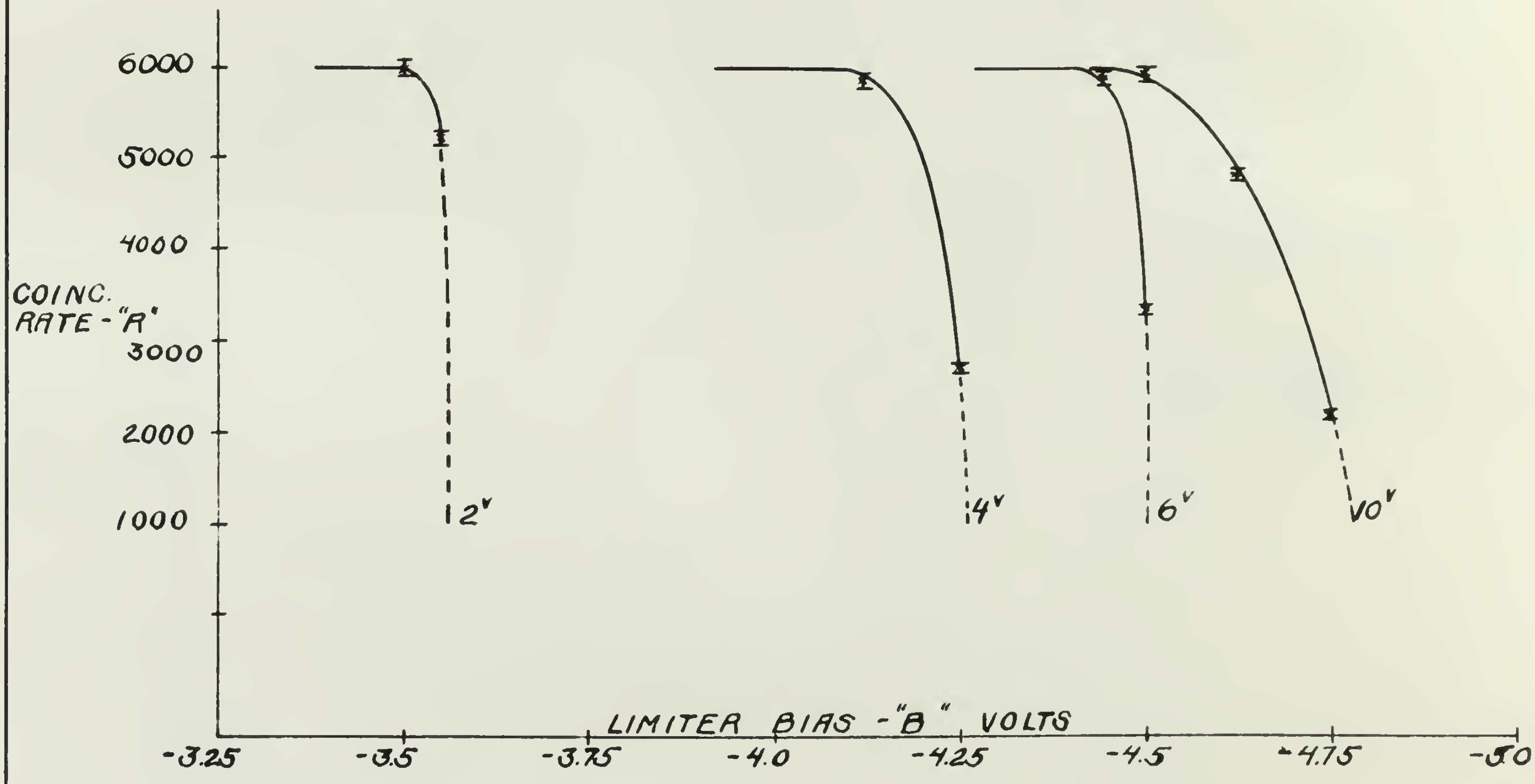

DISCRIMINATOR TESTING - 6BN6 COINCIDENCE CIRCUIT.
COINCIDENCE COUNTING RATE - "R" AS A FUNCTION OF LIMITER GRID BIAS - "B"
PARAMETER - INPUT PULSE HEIGHT IN VOLTS [EQUAL PULSE HEIGHTS ON BOTH LIMITER AND QUADRATURE GRIDS]
QUADRATURE BIAS -3 VOLTS

GRAPH VII-9c

DISCRIMINATOR TESTING
6BN6 COINCIDENCE CIRCUIT

PARAMETER - LIMITER GRID
BIAS - VOLTS

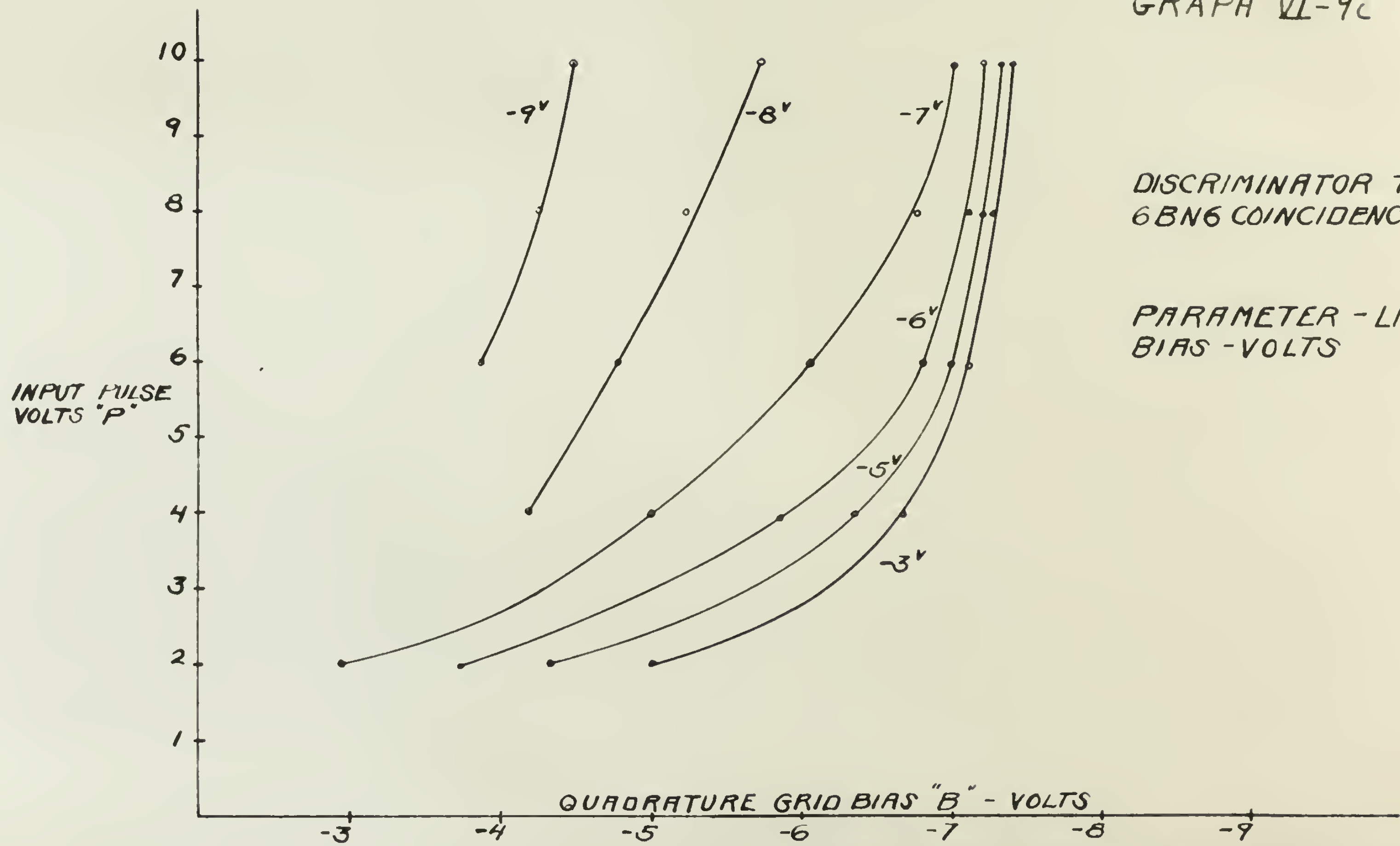

QUADRATURE GRID BIAS-"B" VS. INPUT PULSE HEIGHT (SAME TO BOTH GRIDS) FOR BREAK IN PLATEAU-COINCIDENCE COUNTING RATE.
FOR 90% CUTOFF - ADD ONE (1) VOLT TO GRAPH VALUE.

Thesis Julian 20654
J9 A study of the problems involved in the detection of mu meson pairs from the MIT synchrotron.